Design of stepped frequency continuous wave radars using continuous coherent calibration

by

Dane Robert Thompson

B.S., Kansas State University, 2023

A THESIS

submitted in partial fulfillment of the requirements for the degree

MASTER OF SCIENCE

Mike Wiegers Department of Electrical and Computer Engineering
Carl R. Ice College of Engineering

KANSAS STATE UNIVERSITY
Manhattan, Kansas

2024

Approved by:

Major Professor
Don Gruenbacher

Copyright

Abstract

This thesis details the design of a stepped frequency continuous wave (SFCW) radar known as the Ag Radar (AGR) 120 that operates in the 120 GHz ISM band for agricultural applications. The AGR 120 hardware is centered around a transceiver that integrates transmit and receive antennas, RF mixers, RF amplifiers, and a VCO into a single IC. Due to this high level of integration, significant crosstalk is present in the received intermediate frequency (IF) signals. Methods for removing this crosstalk already exist, such as injecting a correction signal to cancel out the crosstalk prior to sampling the ADC.

In this thesis, the idea of injecting a correction signal is further explored, with the correction signal being continuously derived from the received signal while the radar is pointed at a target. To do this, it is shown that the crosstalk appears as a low frequency signal in the received IF signals which can then be extracted using a low pass finite impulse response (FIR) filter. This creates a feedback loop where the received signal is sampled, a correction signal is derived using the filter, and the correction signal is applied to the received signal of the next sweep of the radar. By introducing this feedback loop, it is shown that the received signal suffers gradual degradation due to noise accrual in the correction signal. As a solution, the correction signal is periodically reset using linear regression with a polynomial model to remove the noise. By using a combination of continuously filtering and periodically resetting the correction signal, the crosstalk is successfully removed while simultaneously receiving target returns.

In addition to describing the continuous coherent calibration technique, this thesis also documents the general design of the AGR 120 including a CAN communication interface that is used for reporting target data and configuring parameters of the radar such as bandwidth and a

method of calculating target distance from the FFT of the received signal using noise thresholding and weighted averaging.

Table of Contents

List of Figures

List of Tables

Acknowledgements

The author would like to acknowledge and thank his major professor Dr. Don Gruenbacher and the committee members Dr. Dwight Day and Dr. Andrew Rys for their time and continued help throughout the author's research and academic career. The author would like to thank Great Plains Manufacturing of Salina, KS for enabling this research with their support. Lastly, the author would like to thank Mr. Garrett Peterson for his mentorship throughout this research and the author's education.

Dedication

Dedicated to my incredible family.

Chapter 1 - Introduction

1.1 Overview of SFCW Radar Systems

As automation and electronic sensing become more popular in consumer and agricultural vehicles and implements, the technology that enables these systems has advanced. One such technology used in these fields is stepped frequency continuous wave (SFCW) radar systems. In general, SFCW radar systems are often used for calculating velocity and distance of physical targets. For example, a SFCW radar can easily be used in the front of an automobile for object detection for cars [1]. For this thesis, the distance calculation of SFCW radars will be the primary measurement considered.

As the name implies, SFCW radars operate by stepping through (sweeping) a range of discrete frequencies to compute distance. From a broad overview, the frequency sweep produces a sinusoid with a frequency related to target distance to be outputted from the SFCW radar in a similar manner to frequency modulated continuous wave (FMCW) radar. This frequency is then computed via the Fast Fourier Transform (FFT).

The application of SFCW radars described in this thesis is for height measurement of towed agricultural implements from the ground. By rigidly fixing a SFCW radar to the implement, distance from the ground can be measured and thus height of the implement relative to the ground can be controlled. In agricultural applications, the environment can become noisy due to excess dust and debris that is kicked up when driving through a field. Due to this noisy environment, radar has a penetration advantage over alternative distance sensor types such as lidar or ultrasonic [2].

1.2 Limitations and Considerations of Small SFCW Radar Systems

For the given application, a physically compact radar system is desirable as it allows the radar to be placed in tight spots in various locations and is cheaper to manufacture. Certain components, such as antennas, have sizes related to operating frequency. To enable a small form factor radar (on the order of 50 mm by 50 mm), a high operating frequency of 120 GHz is used in this research which has a small enough wavelength to allow antennas to be integrated into a single integrated circuit (IC) package. Additionally, wider bandwidths, which increase distance resolution, are easier to achieve at higher frequencies as their fractional bandwidths are smaller. However, due to this high level of integration, unwanted signals caused by crosstalk appear in the received signal. Additionally, close targets such as the focusing lens of the radar can appear as target returns in the received signal. Both the crosstalk and lens returns are unwanted and reduce the amount of gain that can be applied to the received signal without it clipping.

The work in this thesis shows evidence of why calibration to remove these unwanted signals is required for optimal performance and provides motivation for calibrating continuously over time instead of once. It will be shown that calibration with a correction signal that is derived from a return signal including both target returns and unwanted returns is possible with some caveat related to noise accrual in the correction signal. Due to this degradation in the correction signal over time, it becomes necessary to reset the correction signal, which can cause several subsequent sweeps to have poor performance until the correction signal is reconstructed. To minimize the required sweeps needed for a well-calibrated correction signal, this thesis will propose a method of intelligently resetting the correction signal using least-squares linear regression.

1.3 Prior Work

One such method of using a correction signal for removing unwanted signals is known as coherent cancellation calibration [3], [4]. This method proposes pointing the radar at a blank scene, such as the sky, and recording the received signal. Since no targets are present, this received signal captures any unwanted signals and can directly be used as the calibration signal. This method works well and is simple to implement, but it presents some challenges. If the unwanted signals are not consistent between individual radars, such as having different crosstalk characteristics from the manufacturing process, a blank scene must be measured for each individual radar. Additionally, if the unwanted signals change over time, the correction signal must also change over time which can be inconvenient after the radar is installed. Thus, it is desirable to use a correction signal that can be extracted on the fly from the received signal that includes actual targets.

For FMCW radars, [5] proposes using a correction signal extracted from a received signal by using linear regression with a low order polynomial model to approximate the unwanted signals. If the correction signal can be well-represented by a low order, such as a second order, polynomial model, this method can work well. However, if the correction signal requires higher order polynomials, the compute time to perform least-squares linear regression becomes large and thus it would not be practical to compute after each sweep to account for changing unwanted signals.

In this thesis, a method of generating a correction signal continuously and efficiently to allow for continuous calibration that does not significantly reduce the sweep rate of the radar will be proposed.

1.4 Thesis Outline

This thesis contains five chapters in total. The first chapter contains a brief overview of SFCW radars and their role in consumer and agriculture applications. This chapter touches on some issues present in these applications and how they are addressed in the following chapters of the thesis and in previous works. The second chapter describes the operational theory of SFCW radars for distance calculation and how this theory is realized in the Ag Radar (AGR) 120 system developed at Kansas State University. Additionally, the second chapter documents a robust communication interface using the Controller Area Network (CAN) protocol. The third chapter addresses the issues of undesirable signals from crosstalk and lens returns in the received signal of the AGR 120 by proposing a method of continuous coherent calibration and describes algorithms for target detection in the received signal. Next, the fourth chapter shows testing results of the AGR 120 in a field near Manhattan, KS using the methods described in the third chapter. Lastly, the fifth chapter will list the constraints of the proposed methods and describe potential future work.

Chapter 2 - Ag Radar (AGR) 120 Design

This chapter will discuss how a SFCW radar operates and will derive equations that characterize a SFCW radar's range, resolution, and distance for a given target in a returned signal. Then, the hardware and communication interface design of a SFCW radar developed at Kansas State University will be presented.

2.1 Operational Theory of SFCW Radar Systems

As mentioned previously, a SFCW radar sweeps through a frequency range and outputs a signal with a frequency related to target distance. To understand why this occurs, it is important to consider the homodyne transceiver structure used in the AGR 120 given in Figure 2.1 below.

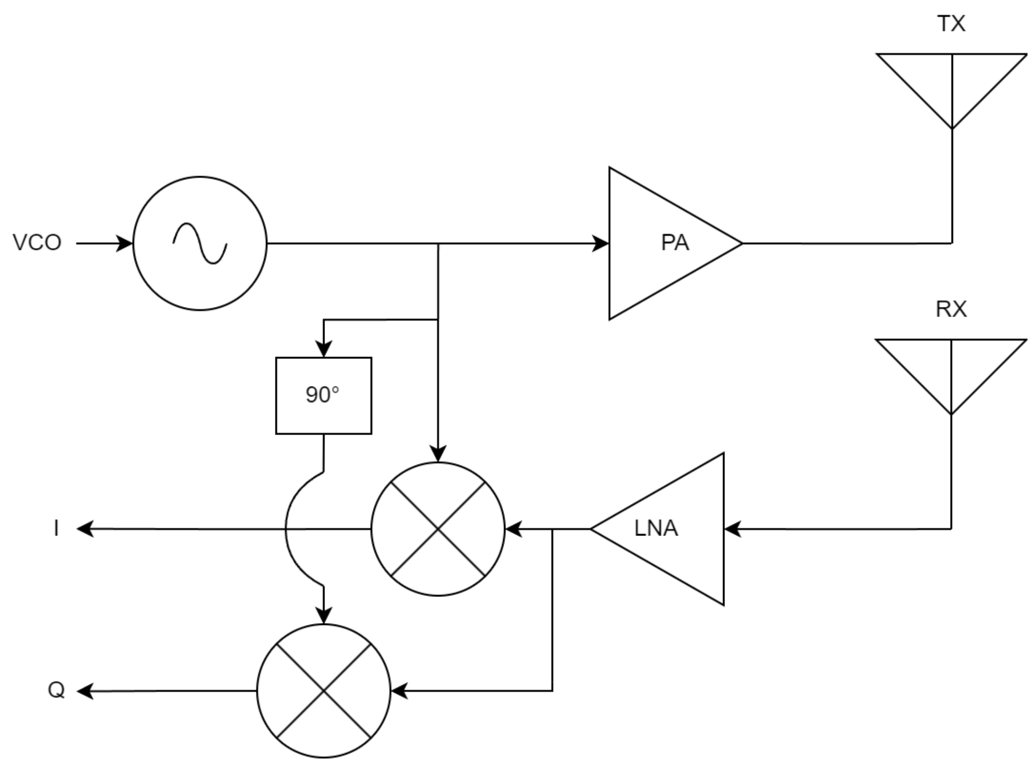

Figure 2.1. Homodyne transceiver diagram.

In a simple case using Figure 2.1, consider a transmitted signal generated by the voltage-controlled oscillator (VCO) that is amplified by the power amplifier (PA) before being radiated towards a target. At the receive antenna, the reflected signal from the target should have the same frequency as the transmitted signal with some Doppler shift if the target is moving and will have some phase offset or delay relative to the transmitted signal due to the time it takes to reach the target and back. At the inputs of the in-phase (I) mixer, the input from the VCO can be represented as $A\cos(2\pi f_{TX}t)$ and the input from the receive low noise amplifier (LNA) can be represented as $B\cos(2\pi f_{RX}t+\theta)$. Using the product to sum trigonometric identity, the output of the in-phase mixer can be calculated using Equation (2.1).

$$I_{mix}(t) = A\cos(2\pi f_{TX}t)\cdot B\cos(2\pi f_{RX}t+\theta) = \frac{AB}{2}[\cos(2\pi(f_{TX}-f_{RX})t-\theta)+\cos(2\pi(f_{TX}+f_{RX})t+\theta)] \quad (2.1)$$

Then, the summed frequency component can be removed using a low pass filter. Thus, the in-phase received output is given in Equation (2.2).

$$I(t) = \frac{AB}{2}\cos(2\pi(f_{TX}-f_{RX})t-\theta) \quad (2.2)$$

Since f_{RX} is simply the sum of f_{TX} and Doppler frequency f_d, Equation (2.2) can then be rewritten as Equation (2.3).

$$I(t) = \frac{AB}{2}\cos(-2\pi f_d t-\theta) \quad (2.3)$$

To relate θ to target distance, it is useful to consider the following definition of phase in a sinusoid where Δt is the time delay from zero phase.

$$\theta = -2\pi f_{RX}\Delta t \quad (2.4)$$

In this case, it can be assumed that the signal being transmitted has zero phase, and Δt can be considered the round-trip time for the signal to reach the target, reflect, and reach the receive antenna. Thus, θ can now be rewritten in a form relating distance d, speed of light c, and the received frequency is then rewritten in terms of transmit frequency and Doppler frequency.

$$\theta = -2\pi\frac{2d}{c}(f_{TX}+f_d) \quad (2.5)$$

For a SFCW radar, each frequency will be sampled once, so the time domain can be written in terms of samples. The transmitted frequency is stepped once per sample, so θ can be expressed as a function of frequency step n.

$$\theta(n) = -2\pi \frac{2d}{c}(f_{TX}(n) + f_d) \tag{2.6}$$

Thus, the value sampled by an ADC is the following where A' is some constant magnitude that can include amplification after the down conversion of the receive antenna signal.

$$I_{ADC}(t) = A' \cos\left(-2\pi f_d t + 2\pi \frac{2d}{c}(f_{TX}(n) + f_d)\right) \tag{2.7}$$

Note, due to the Doppler frequency term, the sample at time t depends on both time and frequency step. If the frequency step is changed at some constant rate F_s with period T_s, then time t can expressed as $T_s n$. Thus, the value sampled by an ADC can be expressed as a function of frequency step as shown in Equations (2.8) and (2.9).

$$I_{ADC}(n) = A' \cos\left(-2\pi f_d T_s n + 2\pi \frac{2d}{c}(f_{TX}(n) + f_d)\right) \tag{2.8}$$

$$I_{ADC}(n) = A' \cos\left(2\pi\left(-f_d T_s n + \frac{2d}{c} f_{TX}(n)\right) + 2\pi \frac{2d}{c} f_d\right) \tag{2.9}$$

Using a similar analysis for FMCW radars in [6], making $f_{TX}(n)$ a triangular ramp with N (typically a power of two for FFT efficiency) discrete frequency values for each side of the ramp allows for removal of the Doppler shift for a given target. To define this, first consider $f_{TX}(n)$ for the up ramp defined in Equation (2.10).

$$f_{TX(up)}(n) = f_{start} + \frac{f_{end} - f_{start}}{N} n = f_{start} + \frac{BW}{N} n \tag{2.10}$$

Note, the bandwidth (BW) is defined as the span between the start and end frequencies of the ramp. Thus, the value sampled by an ADC during the up ramp can now be written as the following equation.

$$I_{ADC(up)}(n) = A' \cos\left(2\pi\left(-f_d T_s + \frac{2d}{c}\frac{BW}{N}\right)n + 2\pi\frac{2d}{c}(f_d + f_{start})\right) \tag{2.11}$$

As shown above, the frequency of this sinusoid is now dependent on distance d and the Doppler frequency f_d. Next, consider $f_{TX}(n)$ for the down ramp defined in Equation (2.12).

$$f_{TX(down)}(n) = f_{end} - \frac{f_{end} - f_{start}}{N}n = f_{end} - \frac{BW}{N}n \tag{2.12}$$

The value sampled by an ADC during the down ramp can now be written as Equation (2.13).

$$I_{ADC(down)}(n) = A' \cos\left(2\pi\left(-f_d T_s - \frac{2d}{c}\frac{BW}{N}\right)n + 2\pi\frac{2d}{c}(f_d + f_{end})\right) \tag{2.13}$$

Using a similar analysis for the quadrature (Q) mixer, the values sampled by an ADC for the up and down ramps are given in Equations (2.14) and (2.15).

$$Q_{ADC(up)}(n) = -A' \sin\left(2\pi\left(-f_d T_s + \frac{2d}{c}\frac{BW}{N}\right)n + 2\pi\frac{2d}{c}(f_d + f_{start})\right) \tag{2.14}$$

$$Q_{ADC(down)}(n) = -A' \sin\left(2\pi\left(-f_d T_s - \frac{2d}{c}\frac{BW}{N}\right)n + 2\pi\frac{2d}{c}(f_d + f_{end})\right) \tag{2.15}$$

To find distance d, the FFT of the up ramp and the down ramp can be computed and normalized by N. When computing a single target, the FFTs should have a large peak at some index k which corresponds to normalized frequency $k/_N$. To compute the FFT of the up ramp, the $I_{ADC(up)}(n)$ will be the real values and the $Q_{ADC(up)}(n)$ will be the imaginary values. Since the frequency of the down ramp is negative, the frequency can be inverted by computing the FFT with $Q_{ADC(down)}(n)$ as the real values and $I_{ADC(down)}(n)$ as the imaginary values. These FFTs produce the Equations (2.16) and (2.17) relating distance and Doppler frequency to the FFT bin frequency.

$$-f_d T_s + \frac{2d}{c}\frac{BW}{N} = \frac{k_{up}}{N} \tag{2.16}$$

$$f_d T_s + \frac{2d}{c}\frac{BW}{N} = \frac{k_{down}}{N} \tag{2.17}$$

To remove the Doppler frequency for a given target found at bins k_{up} and k_{down} in the FFTs, Equations (2.16) and (2.17) can be summed together and divided by two.

$$\frac{k_{up} + k_{down}}{2N} = \frac{2d}{c}\frac{BW}{N} \tag{2.18}$$

Solving for distance d from Equation (2.18) results in Equation (2.19).

$$d = \frac{k_{up} + k_{down}}{2}\frac{c}{2BW} \tag{2.19}$$

Note that if the target is not moving, no Doppler shift will be present (f_d will be 0), thus the target frequency will be the same in both the up and down FFTs. In this case, the resolution of the radar becomes $\frac{c}{2BW}$ and does not depend on the number of frequency values swept (N). Due to Nyquist Shannon sampling theorem [7], the maximum normalized frequency resolvable without aliasing in the FFT is ½. This forces an upper bound on distance (assuming no Doppler shift) as shown in Equation (2.20).

$$\frac{2d}{c}\frac{BW}{N} < \frac{1}{2} \tag{2.20}$$

Solving for distance in this inequality yields the formula for maximum range of a SFCW radar assuming no Doppler shift.

$$d < \frac{c}{2BW}\frac{N}{2} \tag{2.21}$$

2.2 AGR 120 System Overview

To implement this operational theory into a physical design, Mr. Garrett Peterson and I designed a microcontroller-based SFCW radar that operates in the 120 GHz ISM band which will be referred to as the Ag Radar (AGR) 120 throughout this thesis. Mr. Garrett Peterson designed the hardware while I designed the firmware.

The hardware design is centered around the TRA 120 radar front end from indie Semiconductor. This chip features integrated VCO, PA, LNA, mixers, and transmit and receive antennas. Since the VCO operates at an extremely high frequency range (approximately 120 GHz to 126 GHz), it also contains a 1/64 frequency divided output for easier integration with external phase-locked loops (PLLs) that have a smaller frequency range. This front end incorporates the homodyne transceiver design discussed previously in Section 2.1. Thus, the raw radar outputs include separate in-phase intermediate frequency (IFI) and quadrature intermediate frequency (IFQ) components. [8]

The IFI and IFQ outputs are then sent through an amplification stage and sampled by an STM32G474 microcontroller from STMicroelectronics. This microcontroller sports digital to analog converters (DACs), analog to digital converters (ADCs), and programmable gain amplifiers (PGAs), which can all be connected internally [9]. Note, these peripherals will be crucial for the next chapter of this thesis. The microcontroller also controls a TI LMX2491 PLL via SPI to generate frequency ramps. Both acquisition and processing are done with the microcontroller and will be discussed in following chapters of this thesis.

A system diagram of the AGR 120 including the radar transceiver, microcontroller, and assorted miscellaneous components is given in Figure 2.2, below.

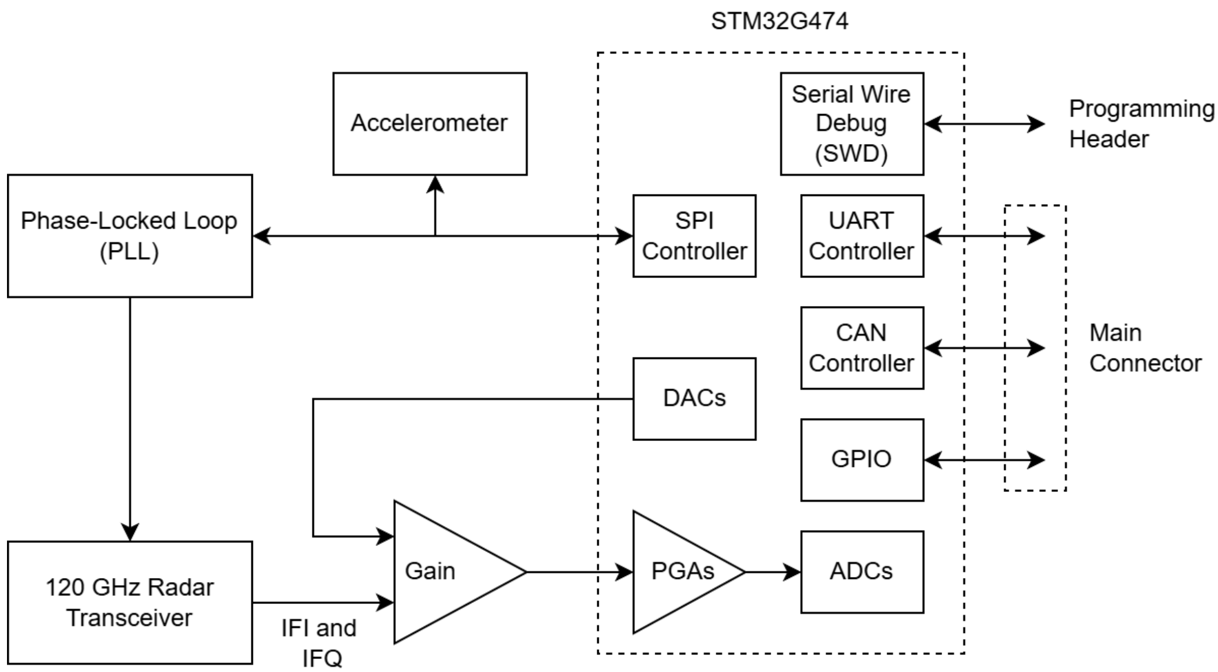

Figure 2.2. System overview of AGR 120.

Figure 2.3, below, shows the assembled AGR 120 printed circuit board (PCB) designed by Mr. Garrett Peterson. It uses a four-layer stackup, is 50 mm by 50 mm in size, and has a waterproof connector to break out power, CAN, GPIO, and UART pins to be used with an external harness.

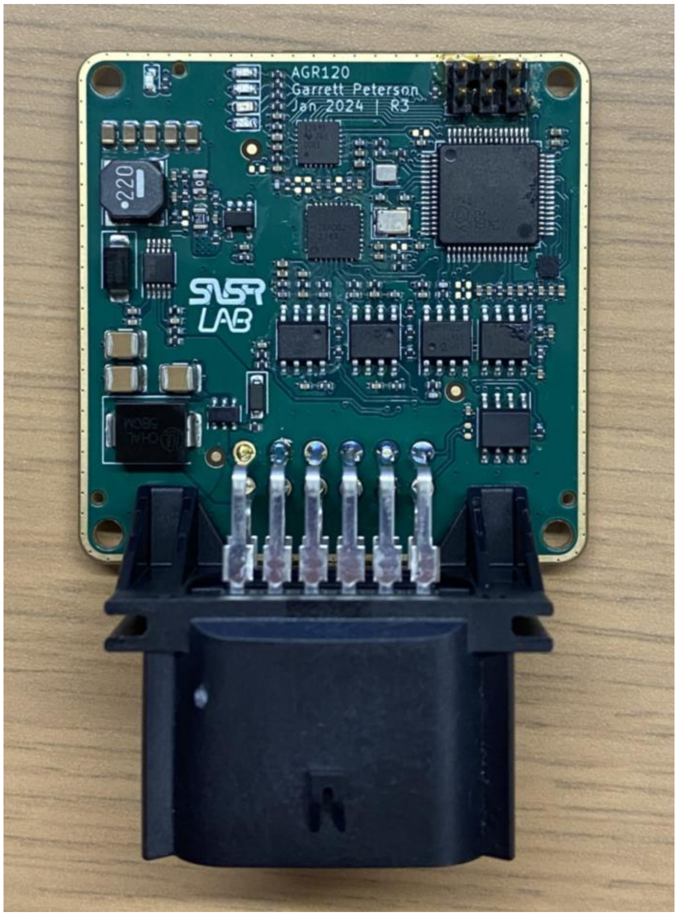

Figure 2.3. Assembled AGR 120 PCB.

To increase the received power of a target’s reflected signal, a focusing lens is used to narrow the beamwidth of the transmitted signal. While this makes the AGR 120 more sensitive to orientation and placement relative to targets, it dramatically increases the received power of near-perpendicular targets, especially at longer distances. The mechanical packaging including focusing lens for the AGR 120 is shown below in Figure 2.4.

Figure 2.4. Mechanical housing and focusing lens for AGR 120.

2.3 CAN Communication Interface

While the AGR 120 is designed to provide distance measurements, several customization options were implemented to tailor the radar for the given environment and application. To control these options and output various measurements, a rugged interface using the Controller Area Network (CAN) protocol was implemented.

CAN is a widely used protocol and comes in many flavors. In the AGR 120's implementation, classic CAN and CAN FD are used. A typical CAN message includes some overhead, which contains an identifier section, in addition to the data being sent. In a typical 11-bit CAN identifier implementation, the identifier for a given message normally indicates the content (or source) of the data being sent and its priority [10]. However, this is usually not enough bits to specify both a source and destination address which would allow for querying. To allow for both source and destination addressing, the CAN interface was designed to use 29-bit identifiers that are similar to SAE J1939 format. The identifier used for the AGR 120 CAN interface uses the format defined in Table 2.1, below.

Table 2.1. 29-bit identifier format for AGR 120 CAN interface.

Bits	**[28:16]**	**[15:8]**	**[7:0]**
Description	Other/Unused	Destination address	Source address

To assign the address of a given AGR 120 unit, three GPIOs (ADDR0, ADDR1, and ADDR2) connected to the microcontroller are assigned logical values at boot via hardware pullups or pulldowns configured in the wiring harness. Once the microcontroller has booted, the CAN source address of the unit is assigned using Equation (2.22), below.

$$AGR\ 120\ Address = Offset + [(ADDR2 \ll 2) \mid (ADDR1 \ll 1) \mid ADDR0] \quad (2.22)$$

The offset value can be chosen arbitrarily such that the address fits in 8 bits. By configuring the address GPIOs, this allows for seven unique CAN addresses that can all be connected to a single CAN bus.

One of the valuable features of the STM32G474 microcontroller is its built-in CAN controller which allows it to natively send and receive CAN messages in various formats such as classic CAN and CAN FD. This CAN controller also includes configurable identifier filtering [9]. By implementing this filter to only allow for CAN messages that use the AGR 120's source address as the destination address, the AGR 120 simply ignores all CAN messages that are not destined for itself. By doing this, multiple AGR 120s ignore each other's transmitted messages when they are connected to the same CAN bus.

This use of addressing and identifier filtering also enables querying the AGR 120 from another device, such as a CAN-connected computer, on the CAN bus. For example, if you wanted to check the orientation after installing a given AGR 120, you could query the on-board accelerometer over the CAN bus and verify that the Z component is near 1G (force due to gravity).

In addition to making queries, it is desirable to configure various options, such as radar bandwidth, using the same CAN interface. The difference between making queries and configuring options can be represented as read (R) and write (W) commands, respectively. To accomplish this, a command structure was formally defined that dictates how data being sent to and from the AGR 120 should be formatted. In this structure, the data format defined in Table 2.2 should be followed when sending messages to the AGR 120.

Table 2.2. Message format used to send CAN commands to AGR 120.

	Byte 0	Byte 1	Byte 2	…	Byte N
Message	Command[0:7]	Payload[byte 0]	Payload[byte 1]		Payload[byte N-1]

If the command being sent does not require a payload, only the command byte needs to be sent. A summary of the defined CAN commands and their expected payloads is given in Table 2.3, below.

Table 2.3. Summary of defined CAN commands and their payloads.

Description	CMD value	Read(R), Write(W)	Payload description	Payload length	Payload format (by bytes)
Configure FFT reporting	0x01	W	Send desired number of targets to return and number of DC values to ignore in peak search	2 bytes	Payload[0] = # of peaks to return (max 2 for classic CAN) Payload[1] = # of DC values to ignore
Request accelerometer data	0x11	R	No payload		
Request temperature data	0x12	R	No payload		
Request electrical health data	0x13	R	No payload		
Request software version	0x14	R	No payload		
Enable FDCAN and set reporting mode	0x15	W	Send flag to configure reporting mode	1 bytes	Payload[0] = 0 for simple, 1 for advanced
Reset unit	0x16	W	No payload		
Reset DAC calibration to constants and configure high or low bandwidth mode	0x17	W	Send flag to configure low BW (122-123GHz) or high BW(120.5-125.5GHz)	1 byte	Payload[0] = 0 for low BW mode (default), 1 for high BW mode

Note, the “Reset DAC calibration” (0x17) command is related to calibration and is relevant to the content in Chapter 3 of this thesis. Another important command is the “Enable FDCAN and set reporting mode” command (0x15). For debug purposes, it is useful to report the raw time series data for a given sweep instead of solely the target distance. The 0x15 command has a payload that configures a simple (default) or advanced reporting mode. The simple reporting mode only reports target distances and their magnitudes. The advanced reporting mode reports the raw IFI and IFQ data for each sweep of the radar. While the simple reporting mode can be done with a single classic CAN message, which has a maximum length of 8 bytes [10], the advanced reporting mode requires more than 8 bytes be sent per sweep as the length of the raw data can be quite long. In this case, CAN Flexible Data-Rate (FD) mode can be enabled on the microcontroller using the 0x15 command which allows message lengths up to 64 bytes [11]. Thus, the sweep can be sent as several 64-byte messages. In the AGR 120’s case, a raw sweep is 532 samples long and contains 2,128 bytes of data as each sample is represented as a 16-bit integer, and both IFI and IFQ have 532 samples. To split the sweep of data into multiple 64-byte messages that can be combined later, the implementation uses the format defined in Table 2.4 and Table 2.5.

Table 2.4. Message format for first 64-byte raw data message in a sweep.

<table>
<tr><td colspan="8">Byte 0</td><td rowspan="1">Byte 1</td><td>Byte 2 – Byte 63</td></tr>
<tr><td>7</td><td>6</td><td>5</td><td>4</td><td>3</td><td>2</td><td>1</td><td>0</td><td rowspan="2">IFI/IFQ PGA gain</td><td rowspan="2">Sweep data</td></tr>
<tr><td colspan="2">Sweep index</td><td>0 = IFI
1 = IFQ</td><td colspan="5">Data index</td></tr>
</table>

Table 2.5. Message format for 64-byte raw data messages after the first message in a sweep.

<table>
<tr><td colspan="8">Byte 0</td><td>Byte 1 – Byte 63</td></tr>
<tr><td>7</td><td>6</td><td>5</td><td>4</td><td>3</td><td>2</td><td>1</td><td>0</td><td rowspan="2">Sweep data</td></tr>
<tr><td colspan="2">Sweep index</td><td>0 = IFI
1 = IFQ</td><td colspan="5">Data index</td></tr>
</table>

In the defined format, the sweep index is a 2-bit counter that identifies which sweep the data is coming from. In most cases, this index is unneeded, but it is useful for stopping a device listening on the CAN bus that has missed messages from combining data that comes from mismatched sweeps. Bit 5 in byte 0 is used as a flag to identify if the data in the message is from the IFI or IFQ channel. The data index is a 5-bit counter that identifies where the sweep data in each message should be placed when reconstructing a single sweep. Note, the data index resets when switching between IFI and IFQ. Both the IFI and IFQ channels have independent PGAs before their respective ADCs, but they are assigned the same gain via software. By reporting this gain value, the sweep can be normalized later. Each value in the raw sweep data is represented as a 16-bit integer and is split into separate bytes using big endian format where the upper byte is sent first in the message.

Chapter 3 - Calibration and Post-Processing

While Chapter 2 of this thesis discusses the operational theory and expected received signal for a SFCW radar, reality is more complicated. In addition to the received signal whose frequency is related to distance, unwanted signals such as crosstalk, noise, and returns from the focusing lens will also be seen at the received signal. This chapter describes these unwanted signals, how to mitigate them, and a method of target distance calculation from the received signal. It should be noted that this chapter will mostly use the IFI channel for analysis, but the same analysis also applies to the IFQ channel and will not be included for brevity.

3.1 Crosstalk and Lens Target Return

Crosstalk is the undesirable interference of a signal with another signal and occurs due to lack of isolation. In the case of the AGR 120 and SFCW radars in general, crosstalk occurs between the transmitted and received signals. As shown in [12], antenna isolation is dependent on both distance separation and frequency. While the TRA 120 does not provide antenna isolation characteristics in its datasheet, it can be assumed that the isolation characteristics are too poor to stop crosstalk as the antennas are placed a short 1.67 mm apart (approximately $\lambda/_{2}$ for 120 GHz) [8]. Additional crosstalk can also occur from other circuitry inside the transceiver [13]. To confirm this crosstalk exists, the AGR 120 was programmed to sweep the transmit frequency while no lens or target was in view. The received signal from the sweep across a low 1 GHz bandwidth from 122 GHz to 123 GHz is given in Figure 3.1, below. Note, a trapezoidal sweep shape is used where the first 256 samples are the up ramp, the middle 20 samples are at a constant frequency, and the last 256 samples are the down ramp. This sweep shape is processed the same as a triangular sweep and will be used throughout the rest of this thesis.

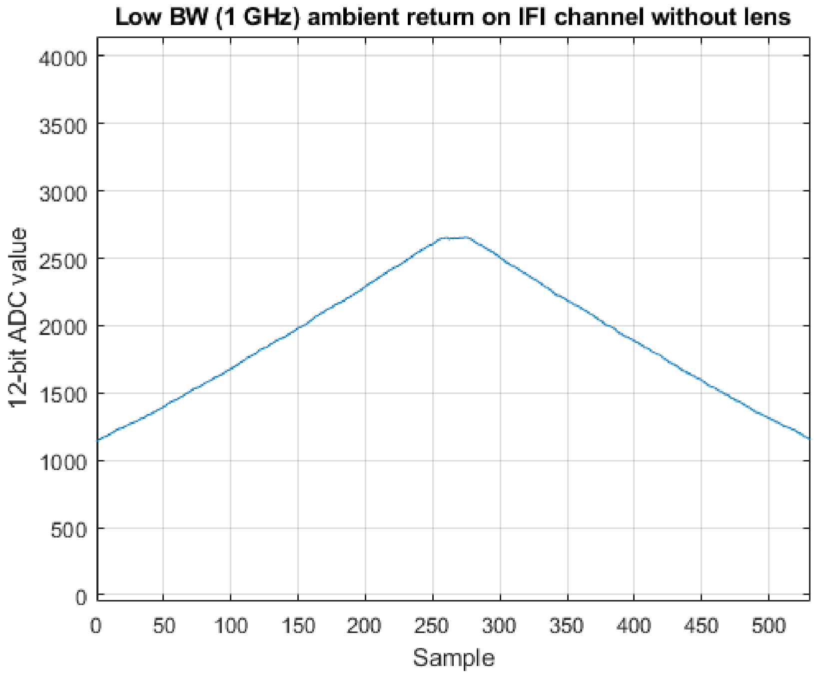

Figure 3.1. Low bandwidth (1 GHz) IFI return with no targets or lens in scene.

This test was repeated for a high 5 GHz bandwidth from 120.5 GHz to 125.5 GHz as shown below in Figure 3.2.

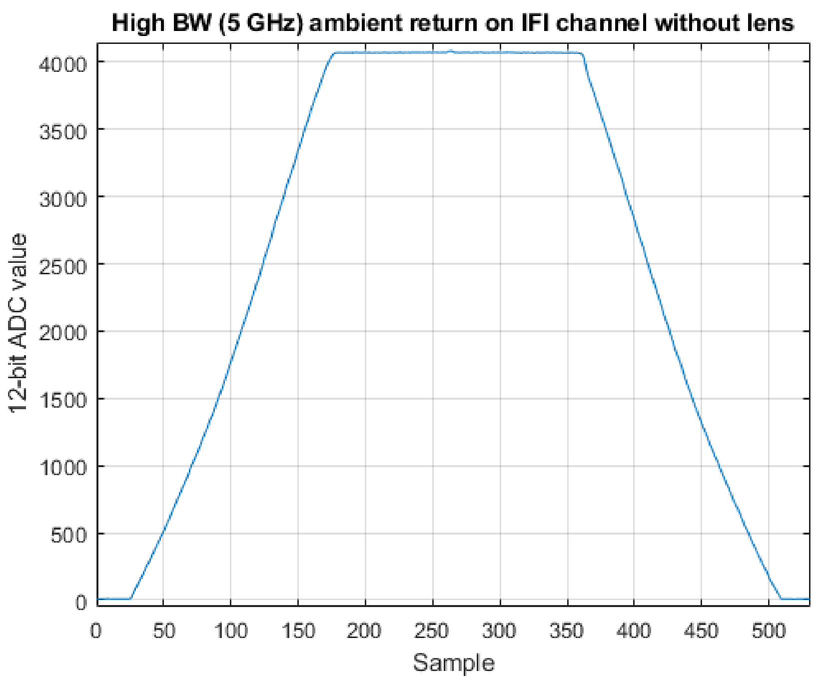

Figure 3.2. High bandwidth (5 GHz) IFI return with no targets or lens in scene.

As shown in the figures above, the crosstalk between the transmitted and received signals is significant. This crosstalk ends up being a large issue as it restricts the amount of gain you can apply to the received signal without the signal exceeding the range of the ADC or PGA. For the high bandwidth example in Figure 3.2, the crosstalk is so significant that the signal is clipped by the range of the ADC and PGA. In an ideal world, the received signal is centered around midscale, allowing a large gain to be applied prior to sampling. In addition to the crosstalk, unwanted targets may be present in the received signal. The most notable unwanted target is actually the focusing lens. Depending on the sweep bandwidth, this distance might be too short to be noticeable, but it can be an issue at higher bandwidths. To show this, the AGR 120 swept through the previous frequencies (low and high bandwidths) with the focusing lens installed. Figure 3.3 and Figure 3.4, below, show the received signal with this test.

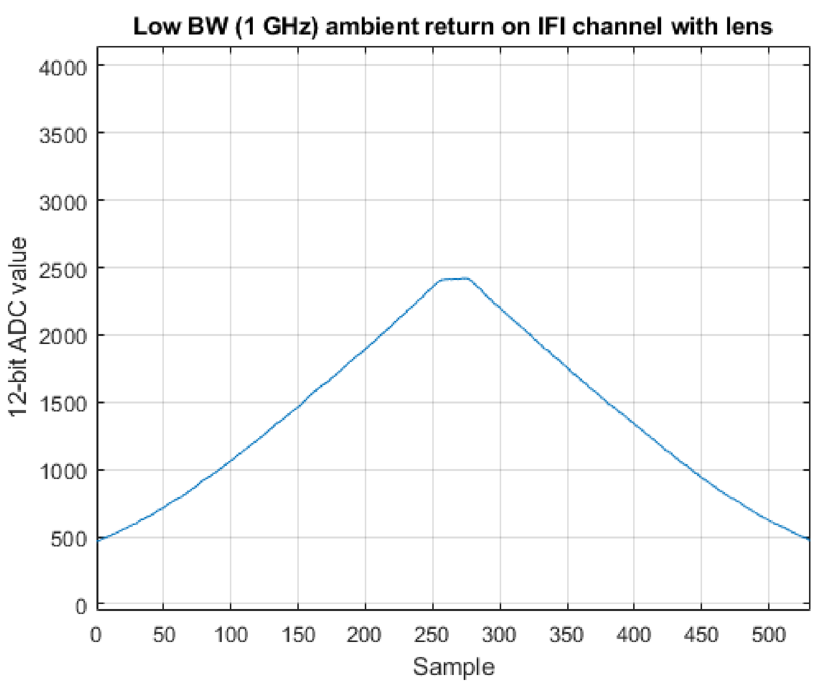

Figure 3.3. Low bandwidth (1 GHz) IFI return with lens installed and no targets in scene.

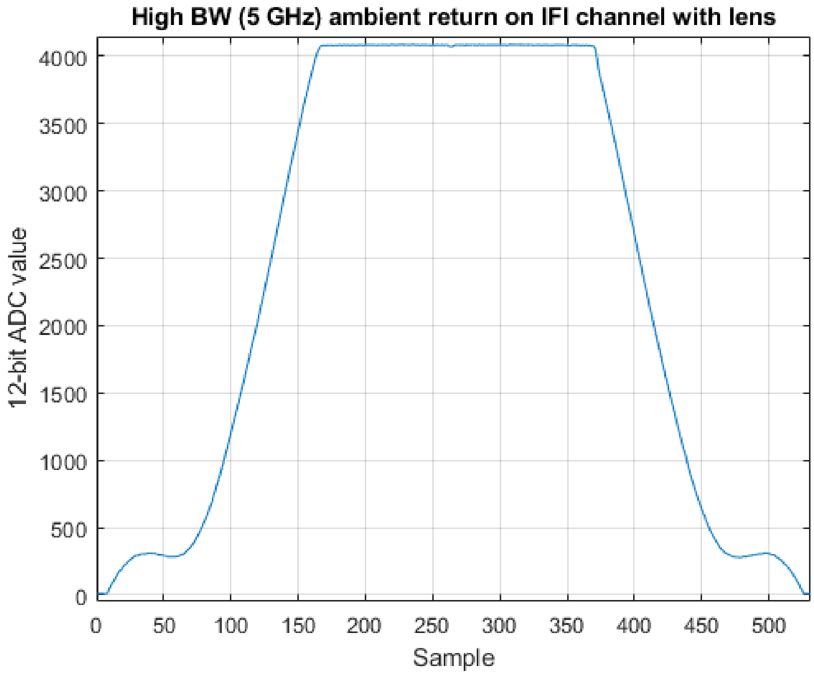

Figure 3.4. High bandwidth (5 GHz) IFI return with lens installed and no targets in scene.

After adding the focusing lens, the high bandwidth IFI return clearly has oscillations near the beginning and end of the sweep. These oscillations are caused by the focusing lens acting as a target and will be exhibited clearly in later parts of this chapter.

An additional behavior more specific to smaller radars is the effect of temperature. The AGR 120 is a small package (50mm by 50 mm PCB) that draws approximately 950 mW during operation. Due to the small package, the board temperature of the AGR 120 can change drastically, especially immediately after turning it on. Thermal images of the AGR 120 PCB in Figure 3.5, below, show dramatic temperature variations on the board after 10 seconds of operation. Note, the hottest areas (the white squares) are the PLL and transceiver IC.

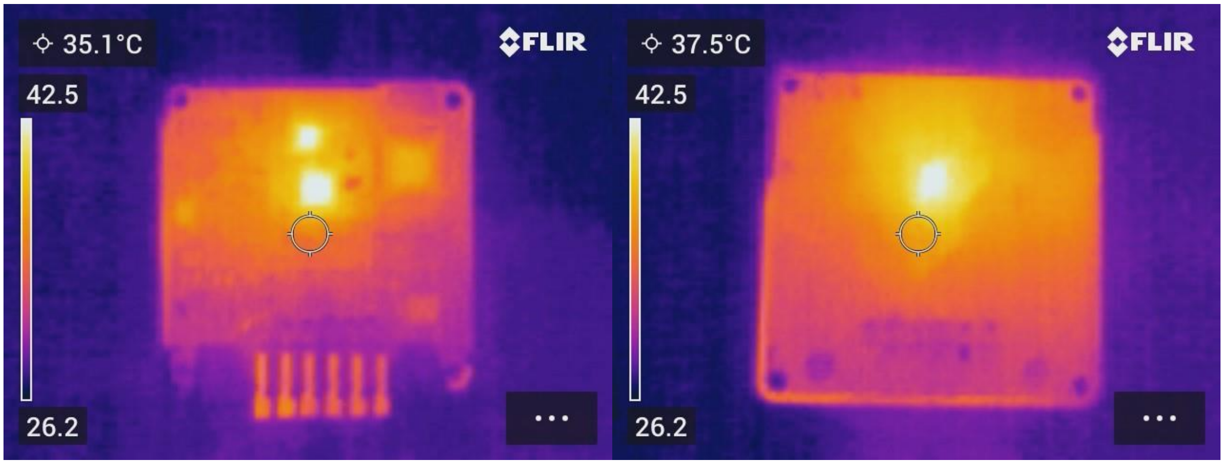

Figure 3.5. Thermal image of top (left) and bottom (right) of AGR 120 PCB showcasing large temperature variations throughout the board.

Since this temperature changes over time as the board heats up, it causes the crosstalk effect to change over time. This effect of temperature over time is shown in Figure 3.6, below.

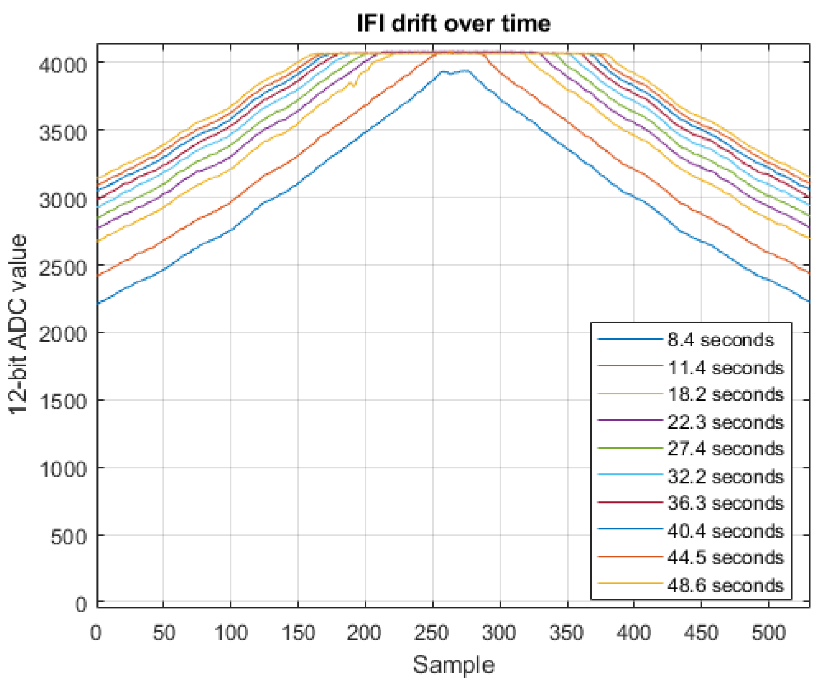

Figure 3.6. Low bandwidth IFI received signal drift over time due to temperature.

As shown in Figure 3.6, the temperature drift can cause the sampled signal to clip after enough time. Because of this transient effect, the previous work using coherent cancellation calibration in [3] and [4] will have issues if the correction signal does not change over time.

However, some sort of calibration is needed to remove the crosstalk and lens return from the received signal. Without this calibration, the gain applied to the IFI and IFQ signals must be low to keep the signal from saturating the ADCs and PGAs. If the signal is calibrated and centered around midscale, more gain can be applied which enables the radar to detect targets from further distances that produce weaker returns.

3.2 Continuous Coherent Calibration

Before exploring the proposed continuous calibration method, it's useful to consider a received signal that includes both the crosstalk, lens return, and an actual target as shown below in Figure 3.7. Note, the target was approximately 44 cm away and the AGR 120 was using a low 1 GHz bandwidth.

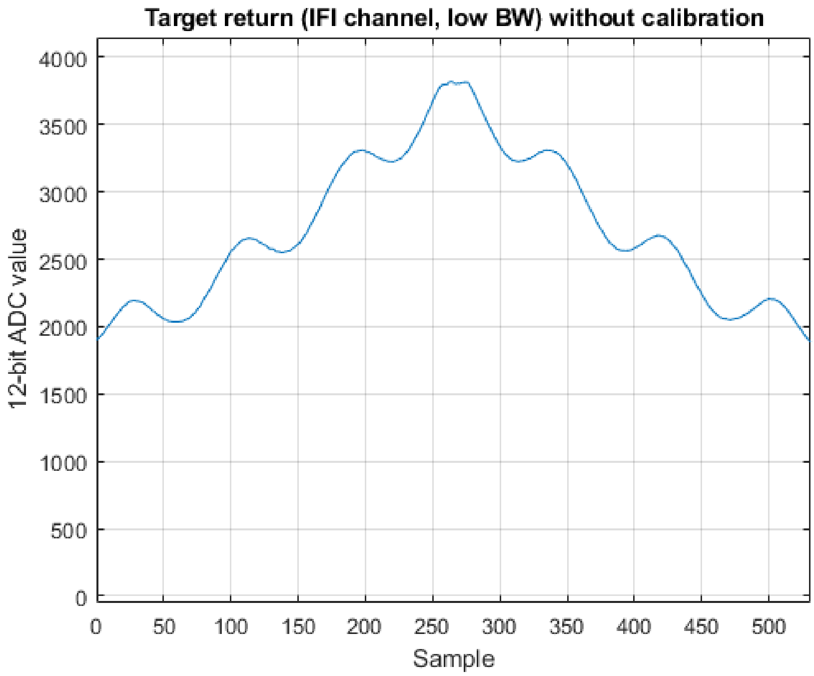

Figure 3.7. Target return on IFI channel in low bandwidth mode without calibration.

From visual inspection, the target of interest has much higher frequency content when compared to the crosstalk and lens return signal. For this application, this will always be true as the range of interest is not close. In general, the higher bandwidth mode crosstalk and lens return signal have higher frequency content than that of the lower bandwidth, but it can be assumed both are still well below the target frequency of interest.

As shown in previous works [3], [4], [5], and [14], it is possible to remove undesirable signals by applying a correction signal, which will be referred to as calibrating. To accomplish this, the design of the amplification and acquisition stage of the AGR 120 should be considered and is shown in Figure 3.8.

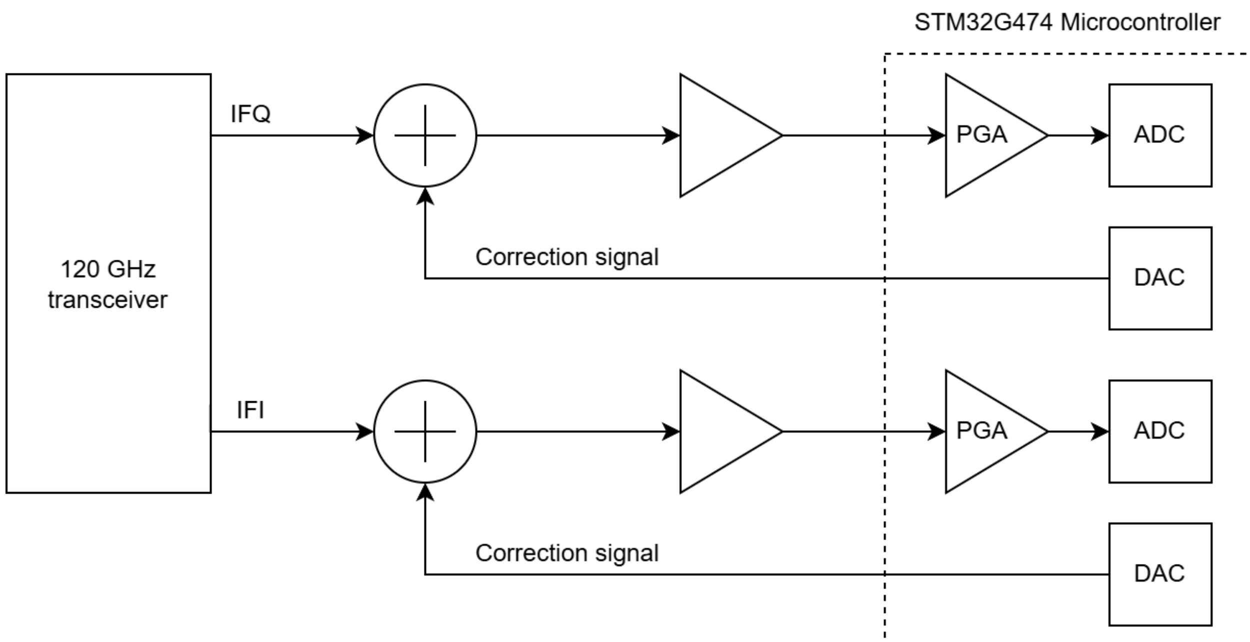

Figure 3.8. Amplification and acquisition stage for sampling IFI and IFQ signals on AGR 120.

For both the IFI and IFQ channels, some correction signal should be applied such that the received signal only contains target returns centered around midscale to allow for maximum amplification. In previous works, the correction signal has been derived from the return of a blank scene such as the sky [3], [4] or a signal derived from a low order polynomial model of the crosstalk [5]. While the blank scene correction is intuitive and simple to implement, this requires manual measurement of the blank scene for each device if crosstalk varies by device and does not account for drift over time. The low order polynomial model could work to remove most of the crosstalk, but it would cause the AGR 120 to suffer from long computation time between sweeps.

It should be noted that an obvious, but unsatisfactory, solution to this problem could be adding a simple high pass RC filter at the IFI and IFQ outputs to remove the low frequency crosstalk and lens return. Since the AGR 120 is designed for a configurable bandwidth, the frequency of the crosstalk and lens return is not fixed, thus a single RC filter designed for one bandwidth will either remove actual targets for other bandwidths or fail to remove the crosstalk and lens return for other bandwidths.

This thesis proposes an alternative calibration method that continuously finds and applies a correction signal while actual targets are in the received signal and will be referred to as continuous coherent calibration. To find this correction signal from a given received signal that includes both targets and crosstalk and lens return, a low pass digital filter is applied to the received signal. Under the assumption that the actual target frequency is higher than the frequency content of the crosstalk and lens return, the output of the low pass filter should be the crosstalk and lens return and will be referred to as the error signal. Then, the difference between this error signal and midscale (2048 for a 12-bit ADC) is computed and added to the correction signal for the next sweep. Thus, over time, the error signal should approach midscale which also corresponds to the received signal being centered around midscale. This creates a feedback loop that operates every sweep and is summarized by the diagram given in Figure 3.9. Note, Figure 3.9 only shows the feedback loop for the IFI channel, but this feedback loop is also implemented separately for the IFQ channel.

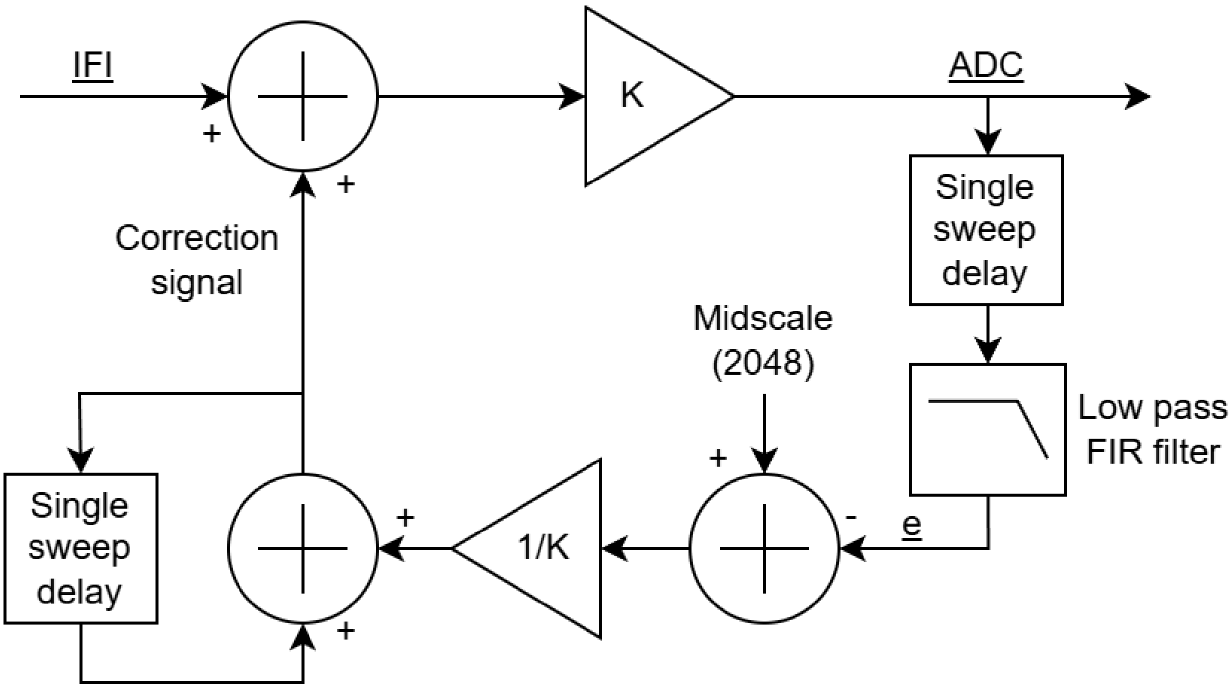

Figure 3.9. Continuous coherent calibration feedback loop using FIR filter.

In the diagram above, each node represents a vector of samples that is the length of the SFCW radar sweep including both up and down ramps. Explicitly, IFI is the IFI signal for a given sweep from the radar transceiver, with each sample in the vector representing a return for a discrete frequency. ADC is the vector of ADC samples for a given radar sweep after the correction signal with the same length as IFI is summed with IFI and some adjustable gain from the external gain stage and internal PGA is applied. The error vector e is the extracted signal including crosstalk and lens return found using a finite impulse response (FIR) filter and is normalized by gain K before being added to the correction signal. Note, the correction signal is initialized as a vector of constants when the AGR 120 is first powered on.

To design the FIR filter for finding the error vector, the hardware was considered first. The STM32G474 microcontroller includes a filter math accelerator (FMAC) peripheral that allows digital filters to be implemented without taking up clock cycles from the main core of the microcontroller. The STM32G474's FMAC has 256 16-bit memory spaces in the peripheral.

These memory spaces are shared between coefficient, input, and output buffers, so assignment of these memory spaces must be done carefully [9], [15]. To determine the corner frequencies of the filter, recall from Equation (2.21) that the maximum range of a SFCW radar is related to the speed of light, bandwidth of the frequency sweep, and the number of steps in the sweep. From this, the FIR filter can be designed in terms of distance instead of frequency which is useful since the low and high bandwidth modes associate distance with different frequencies. For both bandwidth modes, a 101-coefficient FIR filter was made using a least-squares design with MATLAB [16] and was quantized into Q1.15 format for use with the STM32G474 FMAC. While more coefficients could be used, 101 coefficients had a reasonable balance of speed and performance. The responses from these two filters are given below in Figure 3.10.

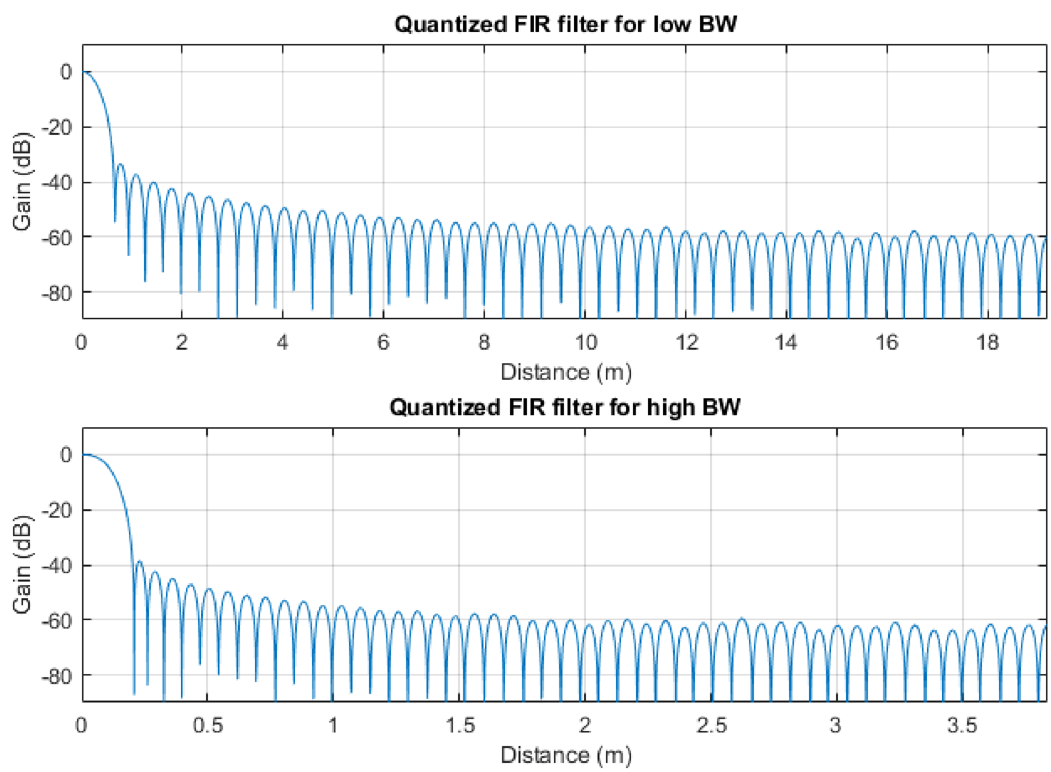

Figure 3.10. FIR filter responses for low (top) and high (bottom) bandwidth modes.

It should be noted that the -3dB cutoff distances (frequencies) are slightly different between the two filters with the low bandwidth filter having a cutoff near 0.25 meters and the high bandwidth filter having a cutoff near 0.1 meters. These cutoffs were chosen through slight adjustment until reaching a satisfactory passband response. Despite these differences, the cutoff distances are shorter than any target of interest for the application of the AGR 120.

To illustrate the effect of these filters, the low bandwidth filter was applied to the signal shown above in Figure 3.7. Note, the signal is padded at the beginning and end and filtered forwards and backwards to achieve a zero-phase filter. The filtered IFI target return in low bandwidth mode without calibration is shown below in Figure 3.11.

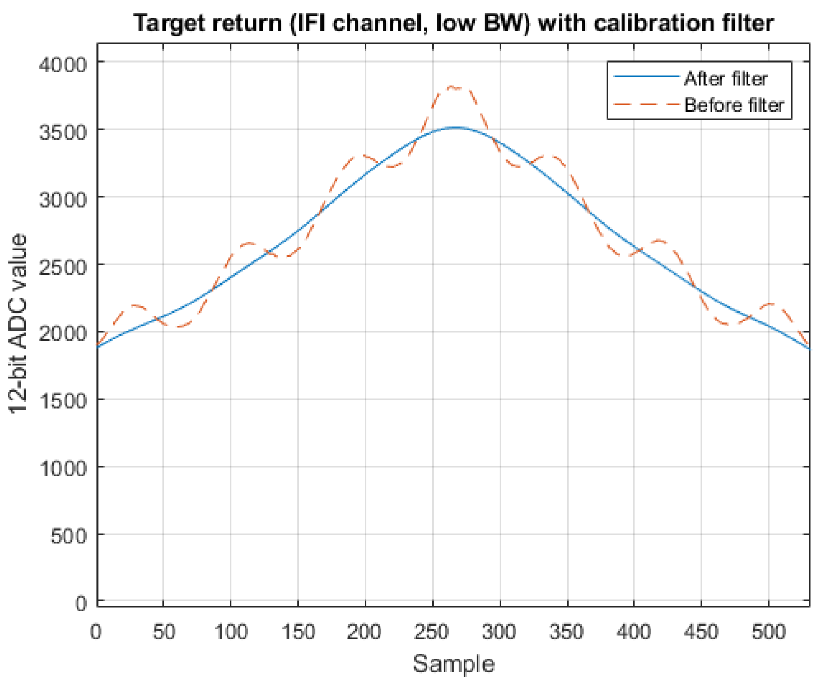

Figure 3.11. Filtered target return on IFI channel in low bandwidth mode.

By applying the filter, the return from the target is clearly removed leaving only the crosstalk and lens return. By using this as the error signal, the correction signal is easily computed by subtracting the error signal from midscale. As an example, this correction signal is calculated and applied to the original return from the target including crosstalk and lens return. In practice, the correction signal will be applied to the return from the next sweep, but reusing the original signal well illustrates the idea as shown in Figure 3.12. Additionally, the error and correction signals used in practice are attenuated to compensate for the gain that will be applied before sampling the ADC.

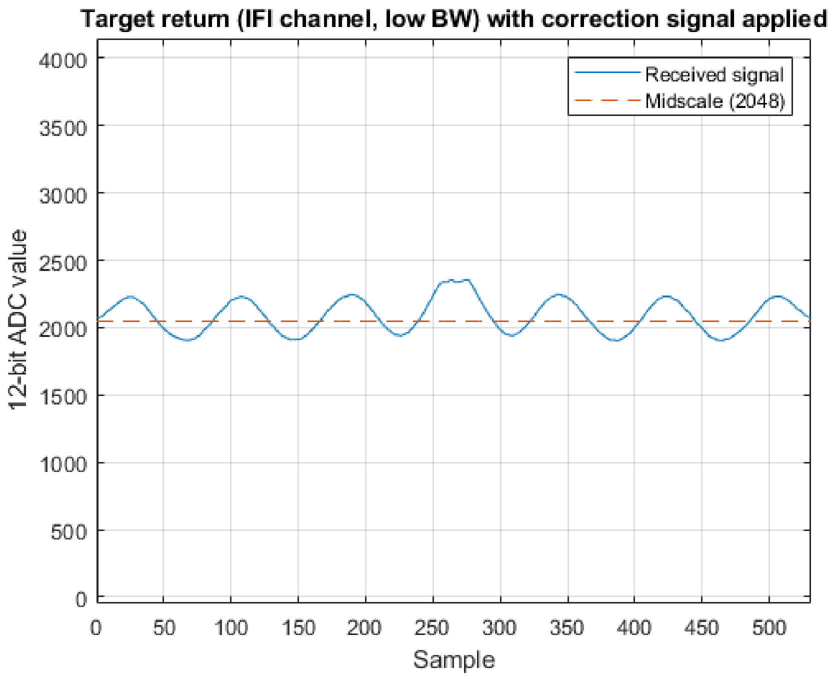

Figure 3.12. Target return on IFI channel in low bandwidth mode with correction signal applied.

After applying the correction signal, the received signal is clearly close to being centered around midscale. When implemented in the AGR 120, this will allow the internal PGAs to have a higher gain without the ADCs or PGAs clipping. In this simple example, the received signal being processed was the same. Next, this strategy was implemented on the AGR 120 to see if the method could be realized. The plot in Figure 3.13, below, shows two returns on the IFI channel at ascending times while the AGR 120 was facing a metal target approximately 1 meter away. Note, each frequency sweep occurs every 206.7 milliseconds in this test. This sweep rate is slower than normal to enable full logging after each sweep.

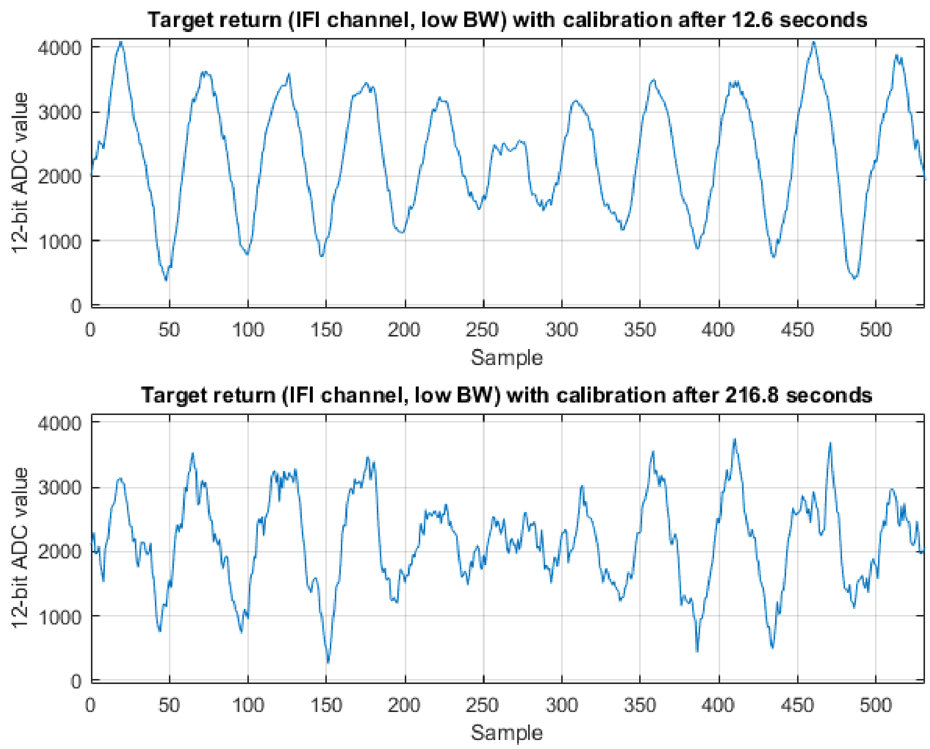

Figure 3.13. Noise accrual in IFI low bandwidth return signal over time.

Clearly, the received signal gradually deteriorates over time and approaches being unrecognizable. By adding the FIR filter into the feedback loop and adding to the correction signal, noise can accrue in the correction signal and is never cleared. To further illustrate this, Figure 3.14, below, shows the correction signals used in the plots in Figure 3.13, above.

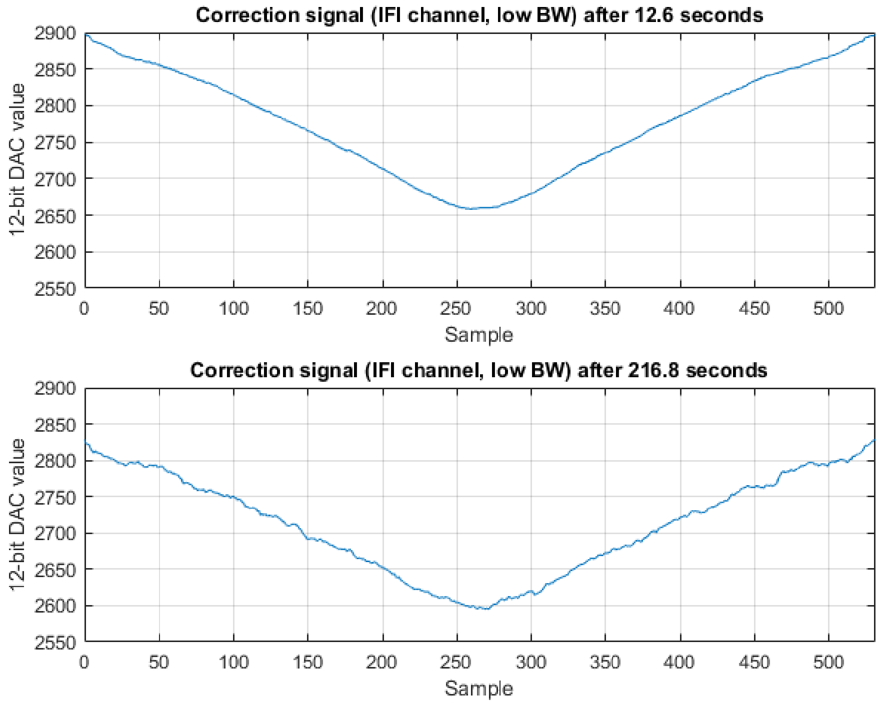

Figure 3.14. Noise accrual in IFI low bandwidth correction signal over time.

Despite the shapes of the correction signals being similar, the small amount of noise present in the correction signal after 216.8 seconds is enough to significantly degrade the signal. Note, small changes in the correction signal can produce large changes at the ADC due to the large amplification stage prior to sampling. Through testing, it seems that this noise grows quicker in the low bandwidth correction signal than the high bandwidth correction signal, but it eventually does affect the high bandwidth correction signal. Additionally, close targets such as waving a hand close to the radar cause the noise to accrue quicker for both bandwidth modes. An example of the high bandwidth target returns after accruing noise is given in Figure 3.15, below.

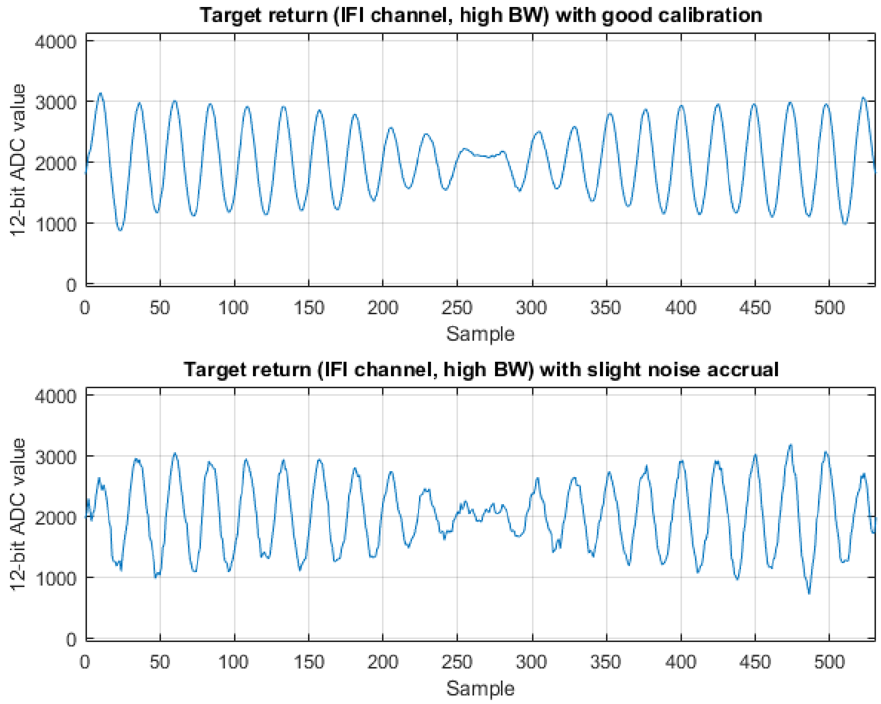

Figure 3.15. Example of noise accrual in correction signal for IFI channel in high bandwidth mode.

While using the FIR filter continuously is optimal for immediately addressing temperature drift and near, undesirable targets, the return signal will eventually become useless as the noise accrues in the correction signal. Despite this unfortunate behavior, there is still some value in the fact that the noise accrues relatively slowly. If the noise takes a significant amount of time (several radar sweeps worth) to become a problem, a method for periodically "resetting" the correction signal is proposed.

When the AGR 120 first powers up, the correction signal is set to a constant value before being updated with the previously described method. Thus, one method of resetting the correction signal is simply assigning it a constant value as done when the AGR 120 powers up. While this would work, several sweeps worth of data will become unusable as the AGR 120 attempts to calibrate itself again. As an alternative, resetting the correction signal to some deterministic signal chosen in an intelligent way is desired.

The proposed method of resetting the correction signal is to split the signal into three equal sections, approximate each section using least-squares linear regression with a polynomial model, and applying a moving average filter to smooth any discontinuities between the three sections. To determine the order of polynomial model to use, the correction signal from the high bandwidth mode should be considered. As shown in Figure 3.14, above, the correction signal from the low bandwidth mode is not very oscillatory, meaning that each section of the low bandwidth correction signal can be well represented by a low, such as a second, order polynomial. The high bandwidth correction signal has more oscillations, especially when the focusing lens is installed as shown in Figure 3.16, below. Note, Figure 3.16, includes minimal noise accrual and is solely used to illustrate the shape of the desired correction signal.

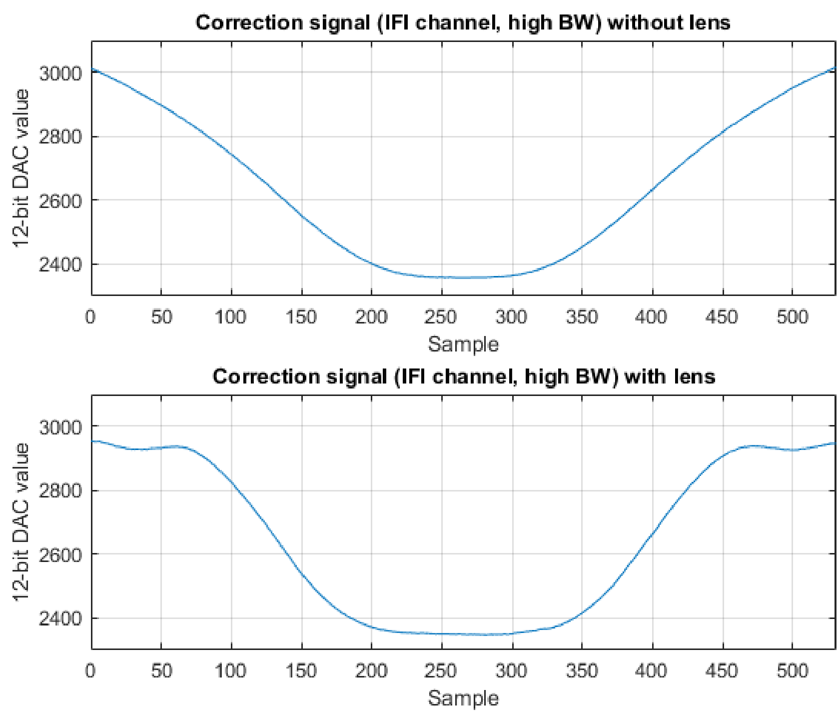

Figure 3.16. High bandwidth correction signal for IFI channel without (top) and with (bottom) focusing lens.

Thus, a second order polynomial model will have difficulty approximating the high bandwidth correction signal. To test this, the correction signals for both low and high bandwidths with noise accrual were approximated using a second order polynomial for three equal length sections of the signal as previously described and smoothed with a 64-sample length moving average filter. By splitting the signal into three sections, a smaller order polynomial can be used to well-capture oscillations than that required if the signal was not split. The results of this test are given in Figure 3.17 and Figure 3.18, below.

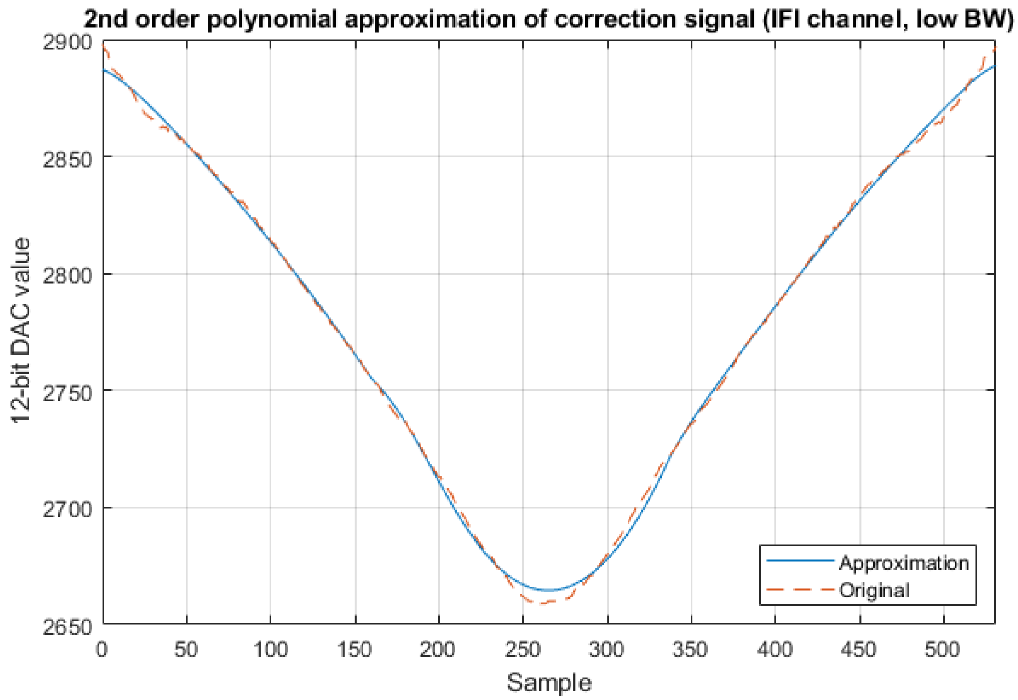

Figure 3.17. Second order polynomial (applied to three sections and smoothed) approximation of IFI, low bandwidth correction signal.

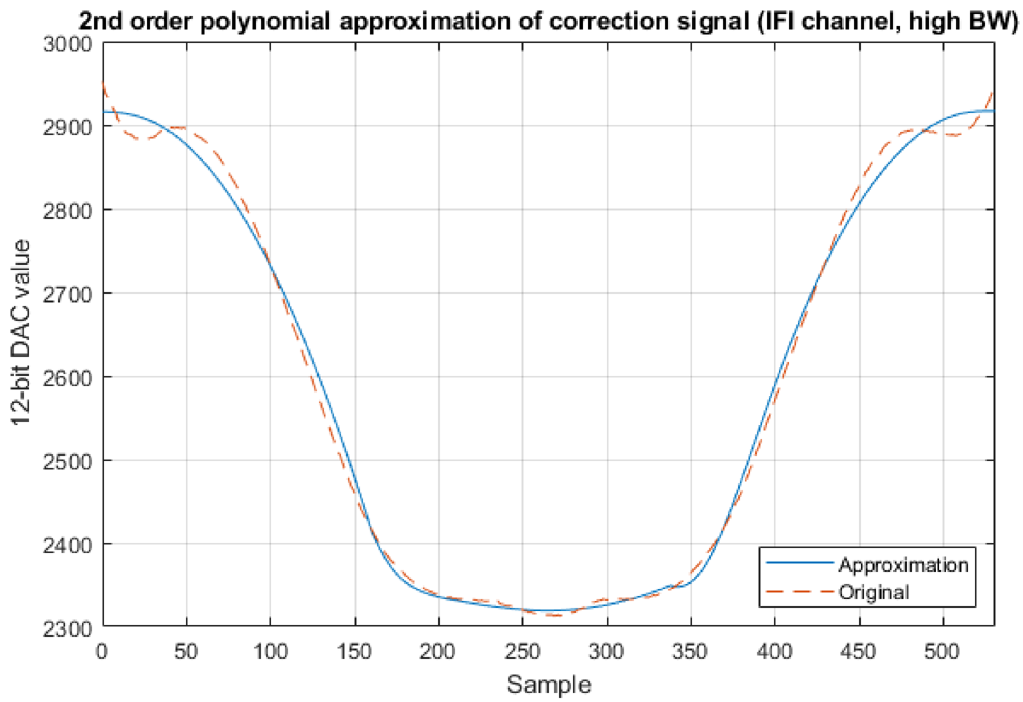

Figure 3.18. Second order polynomial (applied to three sections and smoothed) approximation of IFI, high bandwidth correction signal.

It is shown that the second order polynomial approximation fits the low and high bandwidth correction signals reasonably well. Notably, the approximation for the low bandwidth correction signal slightly mismatches the original near the middle samples of the signal. The high bandwidth approximation mostly matches the original, but fails to capture the oscillations at the beginning, middle, and end of the signal. Higher order polynomial approximations would produce closer matches but will cause a noticeable delay due to the larger number of matrix operations used in least-squares linear regression.

To see the effect of resetting the correction signal using this approximation, Figure 3.19 and Figure 3.20, below, show the received signal before and after resetting the correction signal for low bandwidth and high bandwidth, respectively.

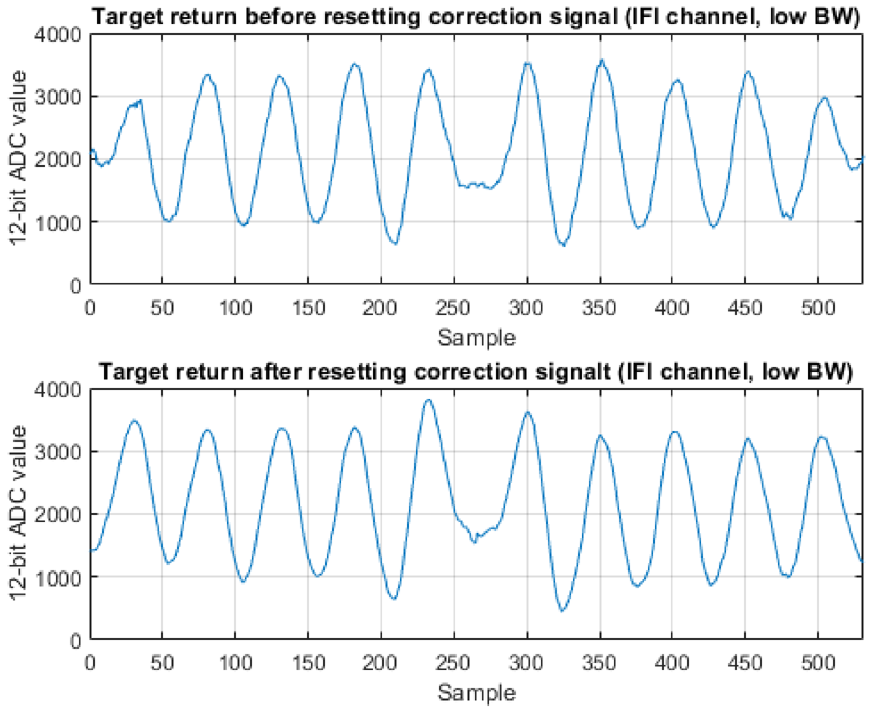

Figure 3.19. Effect of resetting for IFI, low bandwidth correction signal.

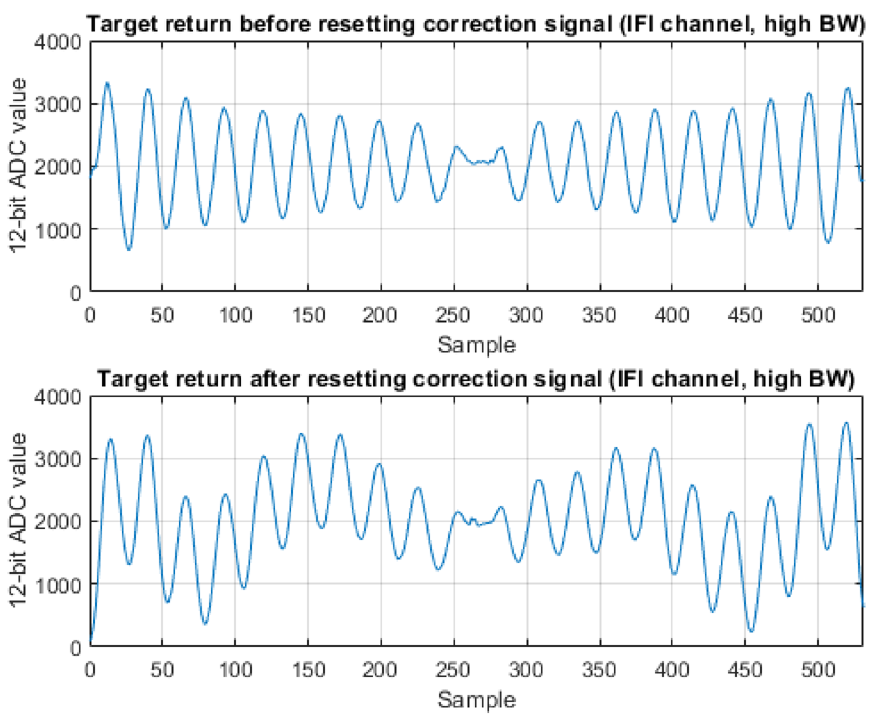

Figure 3.20. Effect of resetting for IFI, high bandwidth correction signal.

As shown above, resetting the correction signal using the second order polynomial approximation results in a near identical correction signal in the low bandwidth case, but a distorted correction signal in the high bandwidth case caused by the oscillations that the approximation did not account for. Fortunately, the approximation is close to correct, which allows the correction signal to be corrected after a couple sweeps using the FIR filter.

As mentioned previously, using a higher order polynomial approximation would result in a better approximation at the cost of compute time. In this case, the time for calibration using the FIR filter and time for resetting the correction signal must be considered and is given in Table 3.1.

Table 3.1. Time between sweeps for different parts of calibration.

Sweep type	Normal calibration using FIR filter	Resetting correction using 2nd order polynomial	Resetting correction using 3rd order polynomial
Time between sweeps	21.9 ms	48.4 ms	214.1 ms

Through testing various targets, it was found that the correction signals typically require approximately five to ten sweeps while calibrating with the FIR filter to become well-calibrated after resetting the correction signal with a series of constant values. Strong, single targets cause the correction signal to require less sweeps to become well-calibrated while weaker and multiple targets cause the calibration to take longer. After resetting the correction signal with the second order polynomial approximation, the high bandwidth correction signal typically needs one or two sweeps while calibrating with the FIR filter to become well-calibrated and the low bandwidth correction signal is usually reset to a well-calibrated state. From a timing perspective, the time to reset the high bandwidth correction signal with the second order polynomial approximation and calibrate with the FIR filter one to two times would result in a calibrated received signal in 70.3 milliseconds to 92.2 milliseconds. If the high bandwidth correction signal is reset to constant values, it could take 109.5 milliseconds to 219 milliseconds to become calibrated using the FIR filter five to ten times. This shows that there is an advantage to intelligently resetting the correction signal using the second order polynomial approximation from a timing perspective. While the third order polynomial approximation typically results in a well-calibrated correction signal for both the low and high bandwidth correction signals, its compute time is too slow to justify over the previous two resetting methods.

Figure 3.21, below, summarizes this method of continuously coherently calibrating the received signal to be centered around midscale and periodically resetting the correction signal using linear regression.

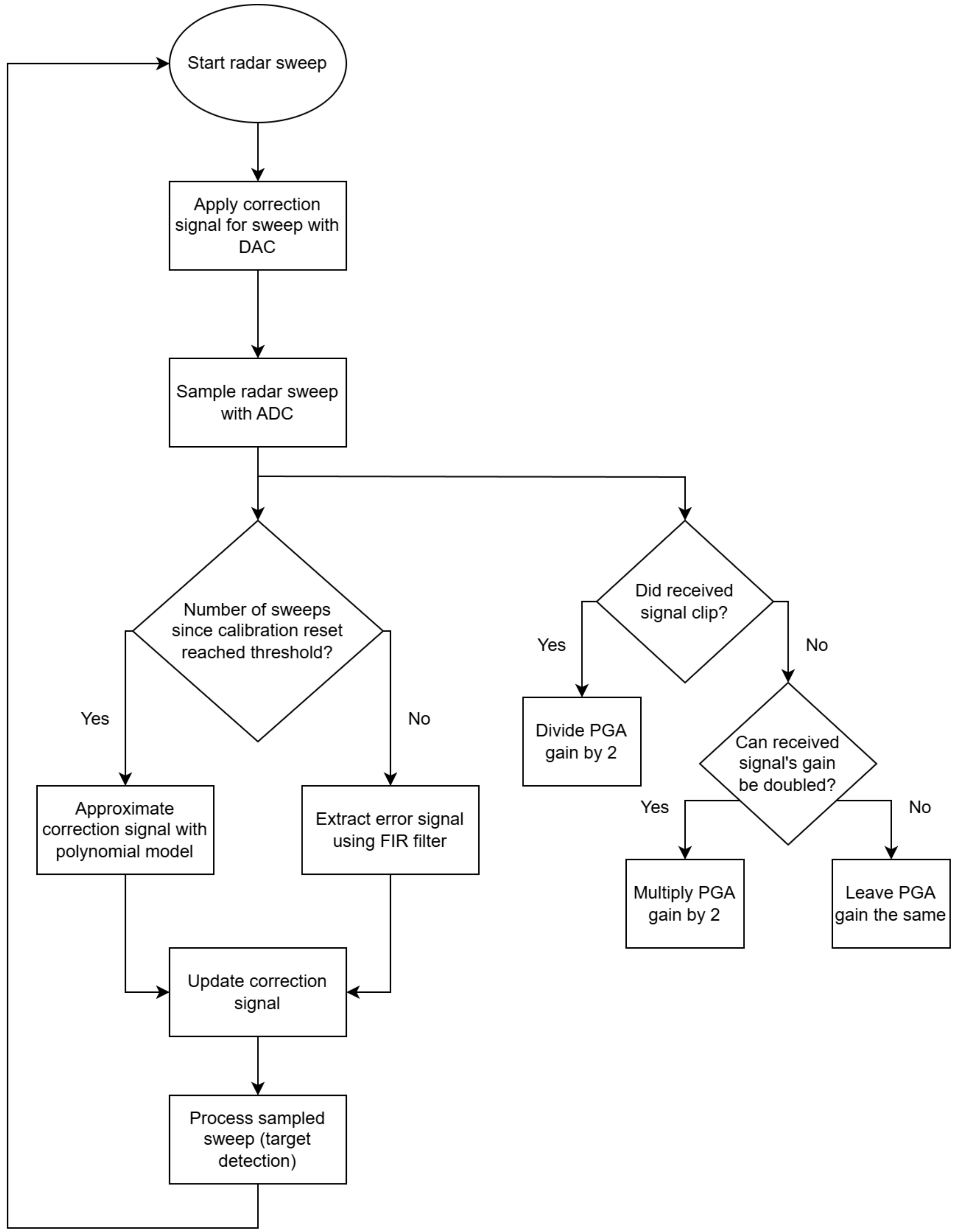

Figure 3.21. Flow diagram of continuous coherent calibration algorithm with periodic correction signal resets and automatic gain adjustment.

3.3 Target Detection

As discussed in Chapter 2, the Fast Fourier Transform (FFT) should be computed after each sweep. Recall from Equation (2.19) that each bin in the FFT represents a distance resolution of $\frac{c}{2BW}$. If a target is at a specific distance, the value in the corresponding FFT bin should be large. As an example, Figure 3.22, below, shows the FFT calculated from a calibrated received signal of the AGR 120 facing the ground at a static distance near 1 meter. Note, the frequency bins on the x-axis are converted to distance and the FFT is computed after subtracting 2048 from both the IFI and IFQ signals to minimize the DC component in the FFT. Additionally, the first bin representing DC is omitted.

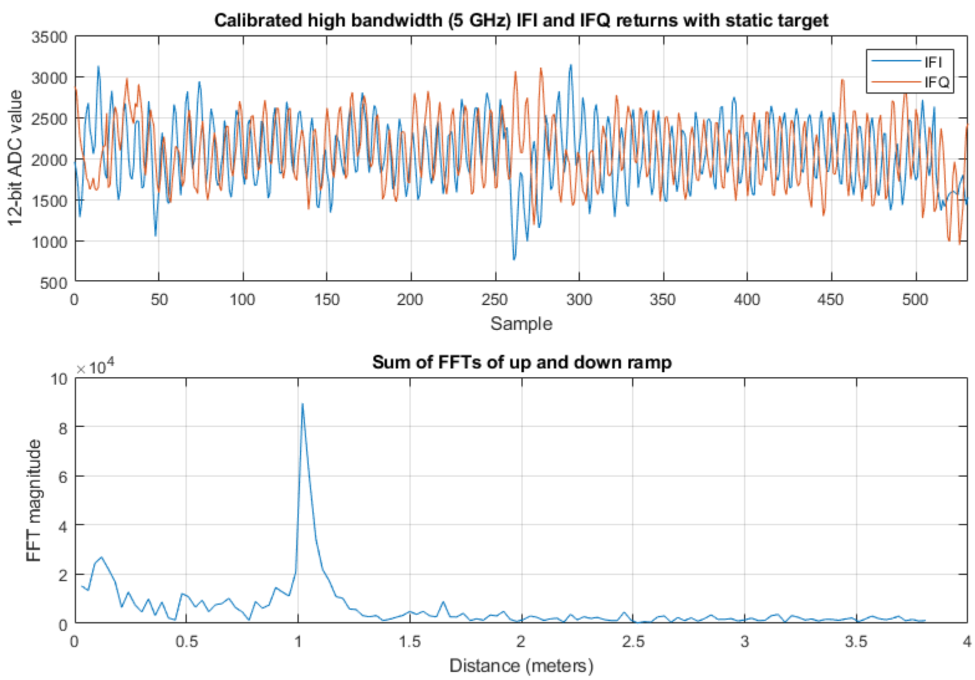

Figure 3.22. Calibrated target returns and their FFT in high bandwidth mode with static target approximately 1 meter away.

In this example, it is clear that the target is near 1 meter and can easily be resolved. In other cases, such as when the target is not as clear, the peak of the target may not be as pronounced relative to the rest of the FFT. This can occur when a target has poor reflectivity or if obstacles, such as vegetation, are between the target and the radar. Additionally, the target may be difficult to resolve immediately after resetting the correction signal as described previously.

Target detection is an extensively researched subject and is not the main focus of this thesis. However, a simple example of single target detection will be provided as the application of this research is for a single target: the ground. To do this, the FFT of a given return signal is computed, then a noise threshold is applied. Any FFT bins with magnitudes less than this noise threshold are set to zero. If the expected distance range is known prior, then the bins corresponding to distances outside of this range [min, max] can also be disregarded. Then, the target distance is computed as the average of the possible target distances weighted by their FFT magnitudes as defined in Equation (3.1).

$$d = \frac{c}{2BW} \cdot \frac{\sum_{i=min}^{max} i \cdot Mag_i}{\sum_{i=min}^{max} Mag_i} \tag{3.1}$$

Using this method with a noise threshold set at 10,000 on the FFT shown in Figure 3.22 and assuming that the target is greater than 0.6 meters away results in a computed target distance of 1.0321 meters.

Chapter 4 - Field Testing of AGR 120

To verify that all the described design strategies work as intended, the AGR 120 was attached to a remote-controllable rover and driven over portions of a soybean field near Manhattan, KS. During this test, the radar was driven over smooth, consistent dirt that had not been worked and an area where the soybeans had been harvested and the crop residue remained. While the radar was being driven, all the raw data was transmitted over CAN using the advanced reporting mode described in Chapter 2. Note, the FFT is computed on the AGR 120, but the results shown here were post-processed using the raw data. Figure 4.1, below, shows the AGR 120 attached to the rover prior to beginning the test.

Figure 4.1. Field test setup with AGR 120 (circled in red) attached to rover.

Once all data had been collected, several series of IFI and IFQ data were left to process. To do this, the FFTs of both the up and down frequency ramps were computed and summed together for each sweep, since the velocity of the ground relative to the AGR 120 was assumed to be near zero. These FFTs were plotted over time as shown in Figure 4.2. Note, the vertical axis is the frequency bins of the FFTs converted to distance, and the bins corresponding to distances less than 0.6 meters are omitted.

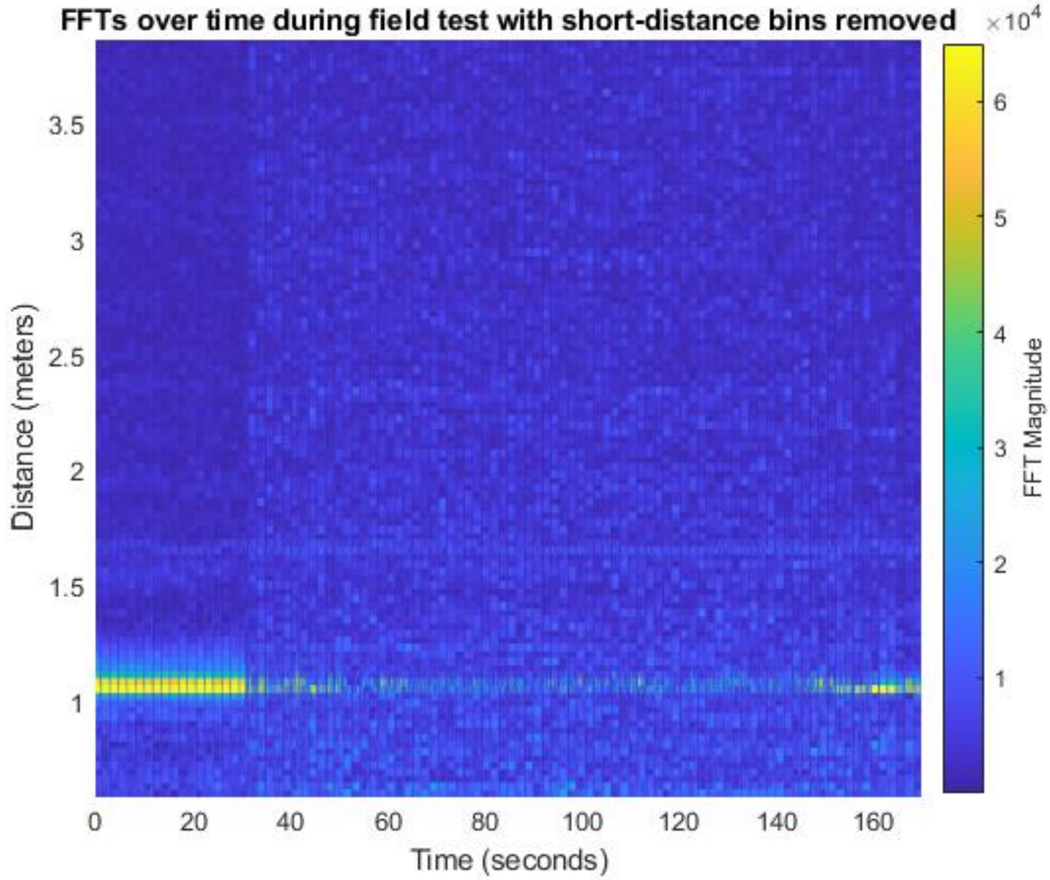

Figure 4.2. FFTs of AGR 120 field test over time. Note, more yellow indicates a stronger target at that frequency (distance).

As shown from this test, the most prominent target in the FFT was slightly above 1 meter and appears as a horizontal line over time. The target is especially strong between 0 and 30 seconds as this is the interval over which the AGR 120 was driven over the smooth, consistent dirt. After 30 seconds, the radar was driven over crop residue and the returns became weaker as the target was less clear. Note, this experiment was a test of some of the methods described in this thesis and should not be used as an indication of performance of the AGR 120. Further improvements to the AGR 120 will be made and are discussed in the last chapter of this thesis.

Despite these weaker returns, a faint horizontal yellow line is still present throughout the length of the test. Using the previously described method of target detection via noise thresholding and weighted averaging, the target distance was computed across time. Figure 4.3, below, shows target distance over time and the target distance over time after applying a 64-sample long moving average filter.

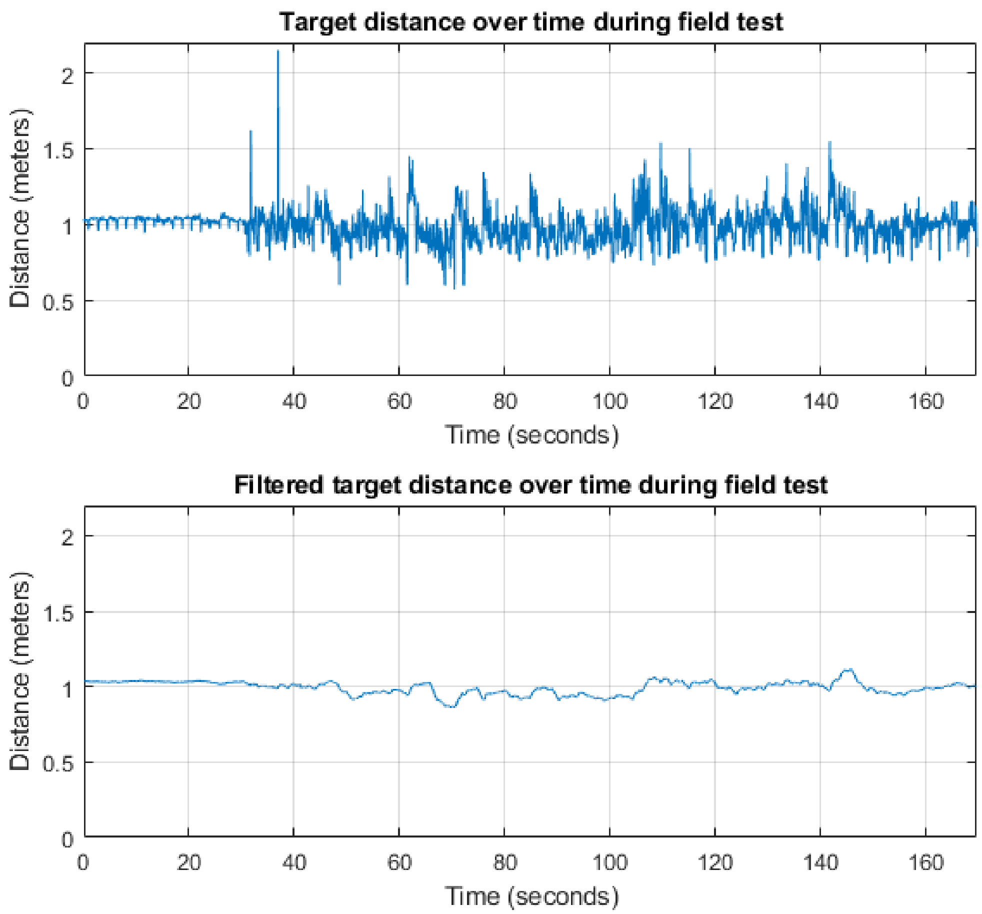

Figure 4.3. Target distance over time during field test without a filter (top) and with a 64-sample long moving average filter (bottom).

As shown above, the calculated distance is very constant (slightly above 1 meter) while the radar is pointed at the consistent dirt then becomes noisier as the rover drives over the crop residue. During the first 30 seconds, brief decreases in the calculated distances on the order of 8 cm occur periodically and are caused by the resetting of the correction signal. However, the target distance can easily be smoothed by applying a moving average filter which results in a much steadier target distance near 1 meter. The variation in the filtered results is reasonable, as the field is not flat and the crop residue is not uniform.

Chapter 5 - Conclusion

This thesis demonstrated that it is necessary and possible to perform coherent calibration continuously on small SFCW radars by extracting a correction signal from a given target return. Issues arose in the form of noise accrual in the correction signal but were addressed by intelligently resetting the correction signal periodically. These methods of calibration were implemented on a physical system and verified for functionality in successfully removing crosstalk and unwanted signals in the received IFI and IFQ signals of the SFCW radar.

With these described methods, several areas can be further explored and improved. In general, the proposed continuous coherent calibration method has several knobs that can be adjusted such as FIR filter cutoff distances, the number of calibration sweeps to allow before resetting the correction signal, and the model used when resetting the correction signal. To truly optimize what these settings should be, more testing is required. While the proposed methods were verified in Chapter 4, their true performance in terms of signal quality was not tested. To fairly test the performance of these methods to alternatives, those alternatives should be implemented on the AGR 120 and compared in a relative manner.

While it was shown that continuous calibration is necessary as the crosstalk can drift over time, it could be more efficient if the system could detect that the correction signal is no longer performing well and perform calibration on a when-needed basis instead of after every sweep. This logic could also be extended to resetting the correction signal by detecting the noise accrual and only resetting the correction signal when the noise accrual grows to some threshold.

In general, the target distance calculation in the field test was reasonable, but other methods are currently being developed and implemented for the AGR 120 to provide more robust distance calculations that provide a confidence level and can handle multiple targets.

Overall, it is hoped that the proposed methods, documented features, and commentary on issues encountered included in this research serve as a solid foundation for those who explore these concepts further.

References

[1] S. Melo *et al.*, "24 GHz Interferometric Radar for Road Hump Detections in Front of a Vehicle," in *2018 19th International Radar Symposium (IRS)*, Jun. 2018, pp. 1–9. doi: 10.23919/IRS.2018.8448029.

[2] J. Vargas, S. Alsweiss, O. Toker, R. Razdan, and J. Santos, "An Overview of Autonomous Vehicles Sensors and Their Vulnerability to Weather Conditions," *Sensors*, vol. 21, no. 16, Art. no. 16, Jan. 2021, doi: 10.3390/s21165397.

[3] G. Peterson and W. Kuhn, "Coherent calibration cancellation for stepped frequency radar systems," in *2018 IEEE Radar Conference (RadarConf18)*, Apr. 2018, pp. 1594–1597. doi: 10.1109/RADAR.2018.8378805.

[4] G. S. Peterson, "A stepped frequency continuous wave short range radar for agriculture measurements with coherent cancellation calibration," Kansas State University, 2020. Accessed: Nov. 03, 2024. [Online]. Available: https://hdl.handle.net/2097/40825

[5] P. Lei, Q. Yu, and J. Wang, "Polynomial Fitting Based Crosstalk Suppression in the Monostatic FMCW Radar," in *2019 IEEE 4th International Conference on Signal and Image Processing (ICSIP)*, Jul. 2019, pp. 284–288. doi: 10.1109/SIPROCESS.2019.8868908.

[6] S. Kim, I. Paek, and M. Ka, "Simulation and test results of triangular fast ramp FMCW waveform," in *2013 IEEE Radar Conference (RadarCon13)*, Apr. 2013, pp. 1–4. doi: 10.1109/RADAR.2013.6586092.

[7] C. E. Shannon, "Communication in the Presence of Noise," *Proc. IRE*, vol. 37, no. 1, pp. 10–21, Jan. 1949, doi: 10.1109/JRPROC.1949.232969.

[8] "indie Semiconductor TRA_120_002 120-GHz Highly Integrated IQ Transceiver with Antennas on Chip in Silicon Germanium Technology." Accessed: Oct. 30, 2024. [Online]. Available: https://downloads.ffo.indiesemi.com/datasheets/Datasheet_TRA_120_002_V0.81.pdf

[9] "Datasheet - STM32G474xB STM32G474xC STM32G474xE." Accessed: Oct. 30, 2024. [Online]. Available: https://www.st.com/resource/en/datasheet/stm32g474cb.pdf

[10] "Bosch Controller Area Network (CAN) Version 2.0 PROTOCOL STANDARD." Accessed: Nov. 03, 2024. [Online]. Available: https://www.nxp.com/docs/en/reference-manual/BCANPSV2.pdf

[11] "Bosch CAN with Flexible Data-Rate Specification Version 1.0." Accessed: Nov. 03, 2024. [Online]. Available: https://tekeye.uk/downloads/can_fd_spec.pdf

[12] C. Trampuz, I. E. Lager, M. Simeoni, and L. P. Ligthart, “Channel crosstalk analysis in interleaved array antennas for FMCW radar,” in *2009 European Microwave Conference (EuMC)*, Sep. 2009, pp. 1345–1348. doi: 10.23919/EUMC.2009.5296232.

[13] K. A. Jenkins, “Substrate coupling noise issues in silicon technology,” in *Digest of Papers. 2004 Topical Meeting onSilicon Monolithic Integrated Circuits in RF Systems, 2004.*, Sep. 2004, pp. 91–94. doi: 10.1109/SMIC.2004.1398175.

[14] P. Smogavec, D. Šipoš, and D. Gleich, “Static and Dynamic Echo Cancellation Algorithm for Ground Penetrating Radar,” in *IGARSS 2023 - 2023 IEEE International Geoscience and Remote Sensing Symposium*, Jul. 2023, pp. 4752–4755. doi: 10.1109/IGARSS52108.2023.10283329.

[15] “STM32G4 - FMAC Filter Math Accelerator Revision 1.0.” Accessed: Nov. 03, 2024. [Online]. Available: https://www.st.com/resource/en/product_training/STM32G4-Peripheral-Filter_Math_Accelerator_FMAC.pdf

[16] “firls - Least-squares linear-phase FIR filter design - MATLAB.” Accessed: Nov. 03, 2024. [Online]. Available: https://www.mathworks.com/help/signal/ref/firls.html